From mean-field hydromagnetics to solar magnetic flux concentrations

Koen Kemel

Cover image: NEMPI in the non-linear stage.
Top: effective magnetic pressure perpendicular to the field (black means negative).
Bottom: concentrations of horizontal magnetic field (yellow) as a result of NEMPI.

ISBN 978-91-7447-576-0

Printed in Sweden by Universitetsservice, US-AB, Stockholm 2012
Distributor: Department of Astronomy, Stockholm University

Abstract

The main idea behind the work presented in this thesis is to investigate if it is possible to find a mechanism that leads to surface magnetic field concentrations and could operate under solar conditions without postulating the presence of magnetic flux tubes rising from the bottom of the convection zone, a commonly used yet physically problematic approach.

In this context we study the 'negative effective magnetic pressure effect': it was pointed out in earlier work (Kleeorin et al., 1989) that the presence of a weak magnetic field can lead to a reduction of the mean turbulent pressure on large length scales. This reduction is now indeed clearly observed in simulations.

As magnetic fluctuations experience an unstable feedback through this effect, it leads, in a stratified medium, to the formation of magnetic structures, first observed numerically in the fifth paper of this thesis. While our setup is relatively simple, one wonders if this instability, as a mechanism able to concentrate magnetic fields in the near surface layers, may play a role in the formation of sunspots, starting from a weak dynamo-generated field throughout the convection zone rather than from strong flux tubes stored at the bottom. A generalisation of the studied case is ongoing.

Acknowledgments

Before hitting the physics stuff, I would like to say thank you to a couple of people who stood by me during the cold dark Swedish winter nights, as well as the more cheery summer barbeques on the Nordita lawn.

First of all there is, of course, Axel, who introduced me to astrophysics,
who guided me when I was trying to get the code to give me sunspots,
who encouraged me when it did not immeditiately do so,
who kept pushing me to write down my findings,
who really likes barbeques.

Then we also have the guys who shared for nearly four years the same office with me, and on occasions cars, planes, trains, hotels, ... Together with whom I conquered turbulence, magnetic fields, suspicious pizzas, snowy Polish mountains, American canyons,...
In order of appearance: Fabio, Simon and Jörn.

Next on my list is Dhruba, a friendly demon overseeing my thesis progress, a great reference for good books both on physics and less serious matters. Thanks for struggling along through the more challenging equations and formulations I encountered in past 2 years.

The Nordita astro group: fellows who came and left again (Alex, Niccolo, Oliver,...), our frequent and long term visitors (Nathan, Igor, Karl-Heinz, Matthias). The rest of Nordita, especially Hans, a social hub and general problem solver.

There were also the other PhD students and the lecturers of the Astronomy department, who essentially tought me all I know about astrophysics, especially Garrelt and my second supervisor Göran.

I don't want to forget my more earth focused friends in Sweden, in Belgium and wherever they moved in the mean time, some people just can't sit still for too long.

Finally, there is my family, both in Belgium: mom, dad, my brother and sister, the cats (who kept my licentiate warm whenever i was away for a bit); and in Sweden: Darya, thanks for ... everything.

List of Papers

The following papers, referred to in the text by their Roman numerals, are included in this thesis.

PAPER I: Brandenburg, A., Rädler, K.-H. & Kemel, K.: 2012, "Mean-field transport in stratified and/or rotating turbulence," *Astron.& Astrophys.* **539**, A35

PAPER II: Kemel, K., Brandenburg, A. & Ji, H.: 2011, "A model of driven and decaying magnetic turbulence in a cylinder," *Phys. Rev. E* **84**, 056407

PAPER III: Brandenburg, A., Kemel, K., Kleeorin, N. & Rogachevskii, I.: 2012, "The negative effective magnetic pressure in stratified forced turbulence," *Astrophys. J.* **749**, 179

PAPER IV: Kemel, K., Brandenburg, A., Kleeorin, N. & Rogachevskii, I.: 2012, "Properties of the negative effective magnetic pressure instability," *Astron. Nachr.* **333**, 95–100

PAPER V: Brandenburg, A., Kemel, K., Kleeorin, N., Mitra, D. & Rogachevskii, I.: 2011, "Detection of negative effective magnetic pressure instability in turbulence simulations," *Astrophys. J.* **740**, L50

PAPER VI: Kemel, K., Brandenburg, A., Kleeorin, N., Mitra, D. & Rogachevskii, I.: 2012, "Spontaneous formation of magnetic flux concentrations in stratified turbulence," *Solar Phys.*, DOI:10.1007/s11207-012-9949-0

PAPER VII: Kemel, K., Brandenburg, A., Kleeorin, N., Mitra, D. & Rogachevskii, I.: 2012, "Active region formation through the negative effective magnetic pressure instability," *Solar Phys.*, DOI:10.1007/s11207-012-0031-8

PAPER VIII: Kemel, K., Brandenburg, A., Kleeorin, N. & Rogachevskii, I.: 2012, "Nonuniformity effects in the negative effective magnetic pressure instability," *Phys. Scr.*, submitted, arXiv:1208.0517

Contents

1. Introduction

You're not the only one
Staring at the sun

Bono, 1997

1.1 Looking at the sun

Galilei published his telescopic observations of dark regions on the solar surface already in the early 17th century (see figure 1.1). These were not the first observations (Vaquero and Vázquez, 2009), but the first of such detail, with a great impact on Western European astronomy. The deeper study of solar activity only started attracting attention in the second half of the 19th century with the discovery of cyclic behaviour in the occurrence of these 'sunspots'. It was Schwabe (1844) who noted in his solar observations 'a cycle with a period of about 10 years'. This is illustrated in figure 1.2 (lower panel) for subsequent observations extending into the present time. The popular response to this discovery was a large quest for phenomena with the same frequency, ranging from geophysical and atmospherical cycles to somewhat dubious demological trends (see also Westwood Oliver, 1883). A more scientific consequence was the discovery and confirmation by respectively Carrington (1858) and Spörer (1883) that sunspot emergence locations move more equatorward as the cycle progresses ('Spörer's law'), shown in figure 1.2 (upper panel).

With the invention of the spectroscope at the beginning of the 19th century, and new insights on the origin of light at the end of the same century, new observational methods became available to astronomers. It became possible to investigate physical properties of faraway objects by analysing their light. One can now measure velocities along the line of sight (Doppler shift), magnetic fields (Zeeman splitting), constituent elements (absorption spectrum), temperature and density. However, the information we can obtain from spectroscopy is limited as we cannot look below the 'surface'. The latter is defined by the radius where the optical depth of the visible continuum spectrum reaches unity. In other words, all information from light emitted below that surface is lost in scattering or absorption, by hydrogen ions (visual) and atoms (UV and X-ray); see e.g. Stix (1989).

Important for the further discussion is the surface velocity field derived from these measurements. We can separate flow structures along different coordinate directions: vertical and horizontal granular flows, polewards 'merid-

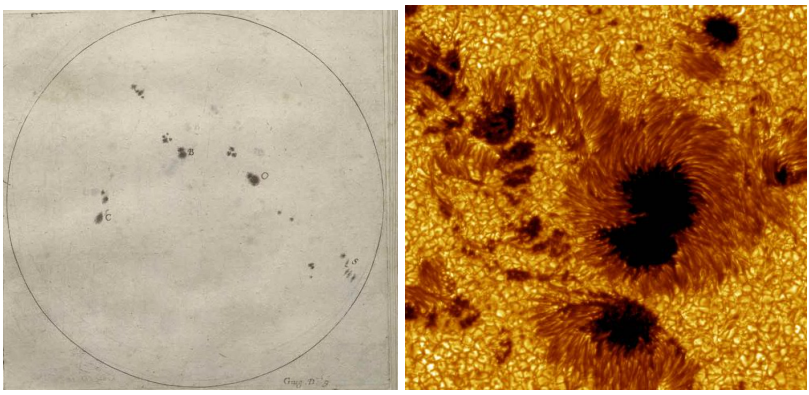

Figure 1.1: Optical observations of sunspots, by Galilei (1613) and more recently with the Swedish 1 m Solar Telescope (Royal Swedish Academy of Sciences).

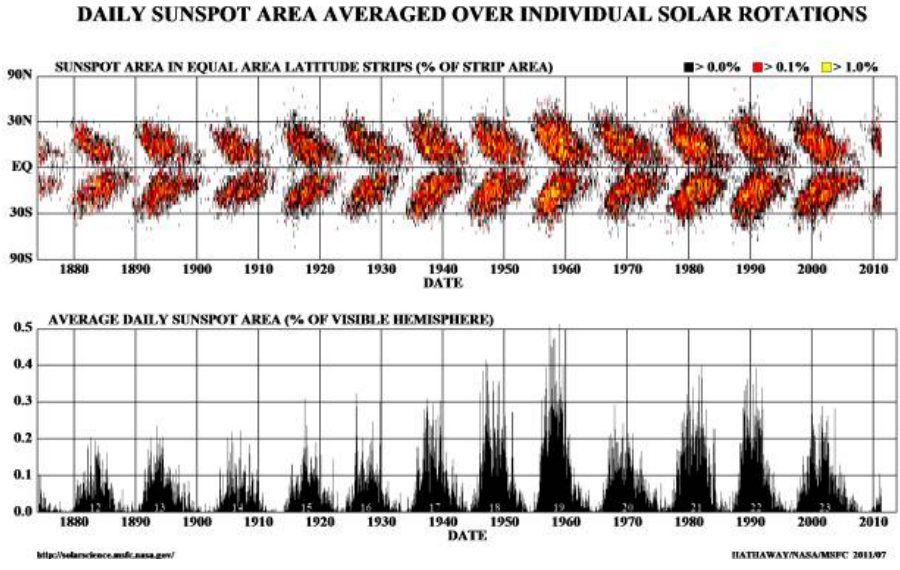

Figure 1.2: Modern data on the number of sunspots (lower panel) and their spread in latitude (upper panel). Taken from NASA/Marshall solar Physics.

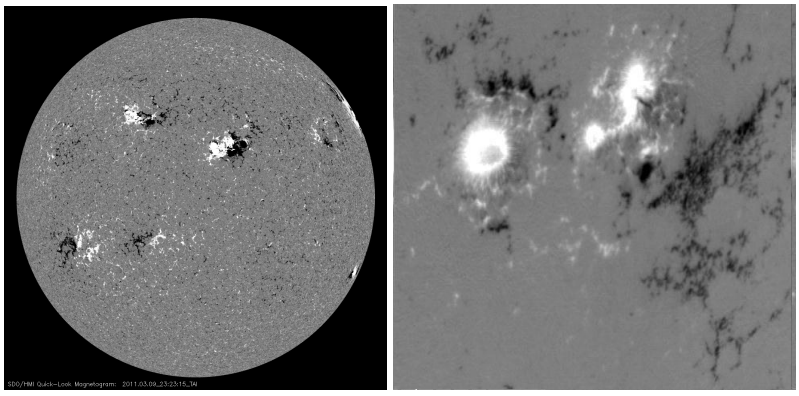

Figure 1.3: Modern observations of magnetic fields (along the line of sight) on the sun: a disc view and an active region (Solar Dynamics Observatory /Helioseismic and Magnetic Imager, SDO/HMI).

ional circulation' and solar rotation. The surface shows differential rotation with a maximum velocity of about 2 km/s near the equator, for more detail see section 1.3. Granulation, convective overturning flows in the photosphere, sets the turbulent scales at the surface: typical values for radial velocities are on the order of 1.5 km/s, cells are between 0.5 and 2 Mm and last for about 10 minutes. Larger supergranules have been detected which can be up to 30 Mm, have a lifetime of about 1.8 days and have a randomly oriented horizontal velocity component with an average of 360 m/s; a more detailed account can be found in Rieutord and Rincon (2010). Meridional circulation is a weak ($\sim$10 m/s) poleward flow (Hathaway, 1996), which is often interpreted to be part of a super cell overturning at the pole down to the tachocline (figure 1.8) and rising up again near the equator. However, as the expected flow velocities are very low, this return flow would be difficult to detect.

1.2 A magnetic sun

In 1896, Zeeman discovered atomic line splitting in a magnetic field (the degeneracy of energy levels is broken by the interaction of the magnetic field with the electron angular momentum), with the secondary lines ($m = \pm 1$ transitions) that are circularly polarised in opposite directions. The combination of a spectrometer and a polarimeter can be used to measure a magnetic field: the wavelength separation of the lines gives a measure of the strength of the magnetic field. This knowledge allowed Hale (1908) to discover the presence of magnetic fields on the solar surface. Examples of modern observations are shown in figure 1.3.

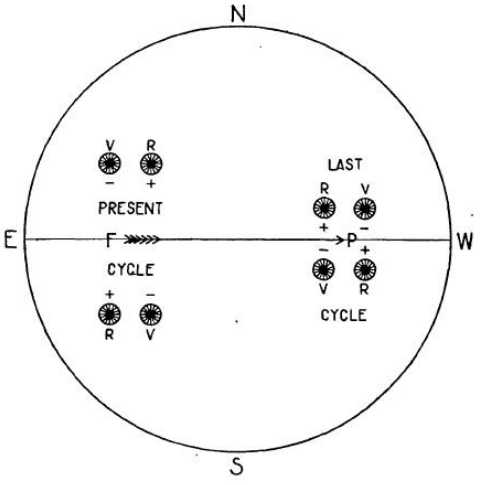

Figure 1.4: Reversal of magnetic polarity of sunspot pairs across the equator and in subsequent cycles, taken from Hale et al. (1919), note also the inclusion of Spörer's law. In the same paper it was also observed that the 'leading' spots (along the direction of rotation) are located closer to the equator ('Joy's law').

These fields come in different strengths and scales. In sunspots the magnetic fields are strong enough (∼3 kgauss) to locally suppress the convective energy flux, making them darker than their environment and thus observable with the naked eye; for an extended observational review see Solanki (2003). Sunspots are relatively small (∼2-20 Mm) and short lived (days to months), which is however much larger and longer than turbulent spatial (∼1 Mm) and temporal (minutes) scales in the surface layers. As mentioned in the previous section, the number and spatial distribution of sunspot occurrences varies with an 11 year cycle. Also, their polarity orientation with respect to the direction of the solar rotation is mirrored across the equator and flips every cycle, as shown schematically in figure 1.4. Sunspots are typically embedded in larger areas (∼100 Mm) of magnetic activity (∼100 gauss for several months). They are referred to as 'active regions' (Martinez Pillet et al., 1997; Yashiro and Shibata, 2001). Finally there is the weak (∼5 gauss) global ($R_{\rm sun}$ ∼700 Mm) solar dipole field, observed only in the second half of the previous century (Babcock, 1959; Babcock and Babcock, 1955). The dipole is aligned with the rotation axis of the Sun and reverses its orientation approximately every 11 years, coinciding with maxima in surface activity at low latitudes; see figure 1.5.

There are modulations in solar activity on even larger time scales, see figure 1.6, to the extent that there can be extended periods without any activity. Ironically the latest 'grand minimum', the Maunder minimum (1650-1750),

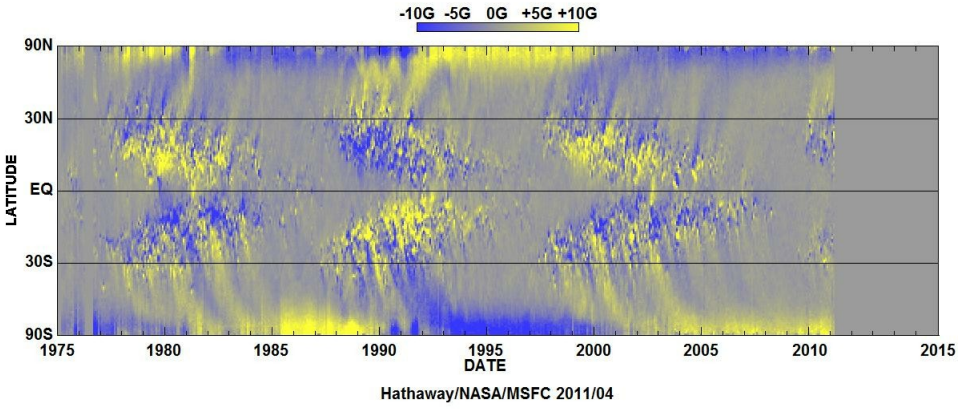

Figure 1.5: Evolution of the weak solar dipole field in the last decades (updated version of a similar figure in Hathaway, 2010).

started a few decades after Galilei's initial observations (Eddy, 1976).

1.3 A peek beneath the surface

As mentioned before, while on the surface we have nearly any information we want with high spatial resolution (~100 km) and reasonable accuracy (for most properties), there are no direct measurements of what is going on below. This is a major obstacle as we want to know where and how the magnetic fields discussed in section 1.2 are formed.

It is, however, possible to obtain some sub-surface information. Helioseismology (Christensen-Dalsgaard et al., 1985; Kosovichev, 1996) is a modern science that studies surface patterns generated by acoustic (pressure) waves in the mHz range propagating in the solar interior. These are the result of the gradual refraction of waves as the sound speed increases (monotonically) with depth, illustrated in figure 1.7. Through inversion of the global surface flow pattern, the radial sound speed profile can be calculated. Combining this profile with a hydrostatic model allows estimation of additional hydrostatic quantities. In addition, advection of these sound waves can be observed as a perturbation in the surface pattern, which gives information about mean flow velocities in the solar interior, provided they are strong enough.

The structure of the sun can be understood in terms of energy transport. In the interior temperatures are high ($\sim 10^7 K$) and therefore the hydrogen opacity ($\propto T^{-7/2}$) is low, which means that heat can be transported through radia-

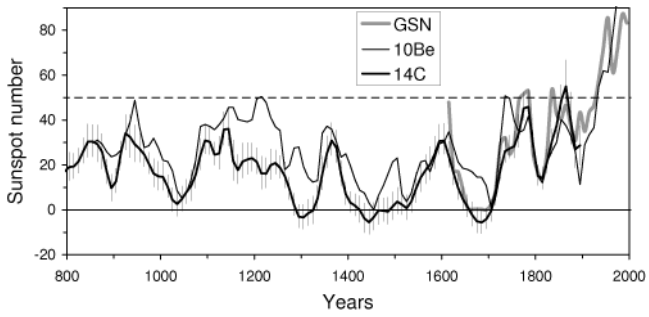

Figure 1.6: Reconstruction of solar activity from observations and isotope abundances in arctic ice (a large number of charged particles results in better shielding of cosmic rays and thus fewer unstable isotopes) agrees well with sunspot counts and shows a large timescale modulation, compared with 10 year averages of the 'Group Sunspot Number'(Hoyt and Schatten, 1998). Figure taken from Usoskin (2008).

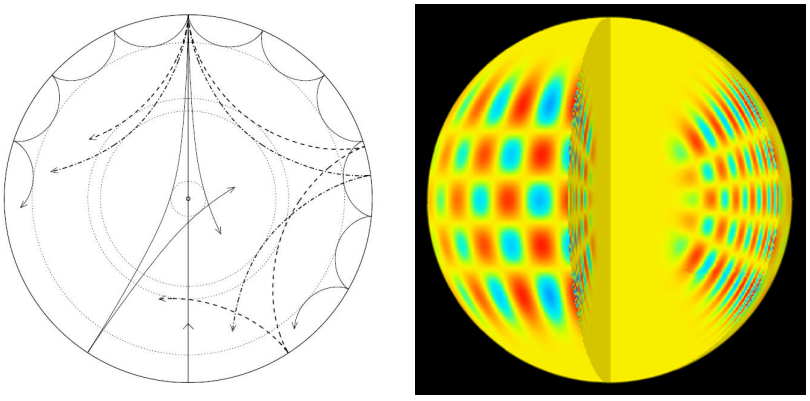

Figure 1.7: The principle behind helioseismology: refraction of waves due to a sound speed gradient (Christensen-Dalsgaard, 2003); the volume reconstruction of a surface pressure wave mode.

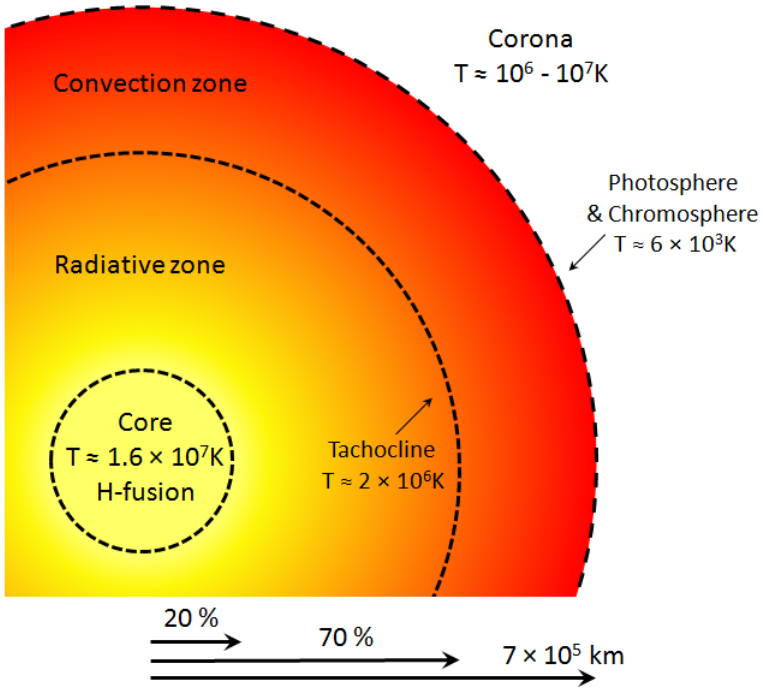

Figure 1.8: Hydrostatic structure of the sun: the core where energy is produced through hydrogen (proton-proton) fusion, the radiation and convection zones in which respectively radiative and convective energy transport dominates and the atmosphere. The latter separates into the photosphere, the thin (~500 km) layer that emits the light we observe in the visible range, the chromosphere, a thicker layer (~2000 km) where the density decreases rapidly while the temperature increases, and the corona, the outer region with very low density and high temperature (Stix, 1989).

tion. As the sun is cooler toward the outer layers, there is a point (~$0.7R_{\text{sun}}$; see Christensen-Dalsgaard et al., 1991) where the opacity becomes high and radiative transport is no longer efficient. In the outer layers of the sun the dominant transport mechanism is convection. Convection yields energy transport through motions without net particle transport: heated dense plasma becomes buoyant (to maintain horizontal pressure balance the density has to decrease) and rises to colder, less dense, layers where it deposits its energy and sinks down again, resulting in laminar cellular flows. The efficiency of this mechanism thus depends on the energy input and the density stratification, requiring a negative entropy gradient.

In the Sun such convective cells, with their size set by the radially decreasing density scale height, can be observed as the granulation pattern at

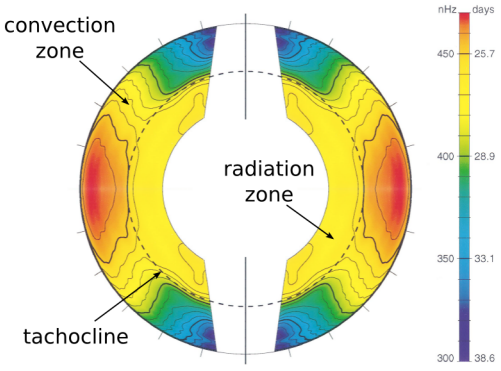

Figure 1.9: Solar rotation profile derived from helioseismology: rigid rotation of the solar radiative zone, spoke-like differential rotation profile in the convection zone with faster rotation near the equator. Taken from Howe (2009).

the surface. Note that, as the viscosity is low, the flows are no longer purely laminar, especially the downflows are expected to be strongly turbulent (Nordlund et al., 2009). The stably stratified regions into which convective motions penetrate at the interface of the convection zone with the radiative interior and the photosphere (again optically thin), are called overshoot layers. The global hydrostatic structure of the sun is illustrated in figure 1.8.

As I will explain later, the important quantity for the generation of magnetic fields is the velocity field. Beside the indication of the presence of turbulence, helioseismology also shows us the large-scale flows (with a net particle transport) in the solar interior. While the radiative interior rotates rigidly, the convection zone rotates differentially in a spoke-like pattern: increasing angular velocity outwards and towards the equator, shown in figure 1.9. Steeper velocity gradients occur near the surface and at the transition between radiative interior and the convection zone, the latter shear layer is named ‘tachocline’, while the former one is called the ‘near-surface shear layer’.

In local helioseismology, rather than using global patterns, one looks at a specific area to determine the flow field directly below the surface. Such measurements indicate that the flow disturbances due to sunspots are relatively shallow; see figure 1.10. To conclude this section I would like to stress that there are no direct or indirect measurements of magnetic fields below the surface.

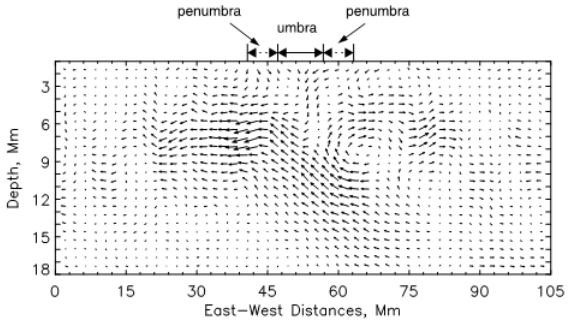

Figure 1.10: Reconstruction of the flow around a sunspot from local helioseismology data. Taken from Zhao et al. (2001).

1.4 Where do those fields come from?

To answer this question we need an understanding of the interaction between magnetic fields and turbulence. We studied, on one hand, the effect of turbulence on the evolution of magnetic fields (Chapter 2), applied to astrophysics (**Paper I**) and lab plasmas (**Paper II**) and, on the other hand, the effect of a mean magnetic field on turbulence (Chapter 5). This study was performed mostly through numerical simulations, described in Chapter 3.

It is clear that the global solar field, oscillating with a period of about 22 years, is generated through a dynamo mechanism (the conversion of kinetic to magnetic energy). The 'standard model' (Fan, 2009) assumes a strong magnetic field stored at the bottom of the convection zone, amplified through shearing in the tachocline. This field rises to the surface in the form of magnetic flux tubes, forming the observed bipolar magnetic structures as they pierce the surface. Residual poloidal magnetic fields (the leading spot tends to lie closer to the equator ('Joy's law'), thus giving a small poloidal component) are transported polewards by the meridional flow, contributing to the dipole field. While elegant, this model does make a number of strong assumptions and does not always agree with observations (see Chapter 4).

The main idea behind the work presented in this thesis is to investigate if it is possible to find a different mechanism that leads to surface magnetic field concentrations that could operate under solar conditions and which does not postulate the presence of flux tubes rising from the bottom of the convection zone. In this context we study in Chapter 5 the 'negative effective magnetic pressure effect': it was pointed out in earlier work (Kleeorin, Rogachevskii, and Ruzmaikin, 1989) that the presence of a weak magnetic field can lead to a reduction of the total turbulent pressure. This reduction is now indeed clearly observed in simulations (**Paper III**). As magnetic fluctuations experience an

unstable feedback through this effect, this leads, in a stratified medium, to the formation of magnetic structures, first observed numerically in **Paper V**. While our study setup is relatively simplified, one wonders if this instability, as a mechanism able to concentrate magnetic fields in the near surface layers, may play a role in the formation of sunspots, starting from a weak dynamo-generated field throughout the convection zone rather than from strong tubes stored at the bottom. The properties of the turbulent pressure reduction and the instability were studied more thoroughly in the remaining papers. In particular, in **Paper IV** we show that three-dimensional instabilities only need to be considered if the negative effective magnetic stress is also negative, which is however not the case in the models studied so far. In **Paper VI** we compute the convergence of the parameters describing the negative effective magnetic pressure as a function of magnetic Reynolds number, and in **Paper VII** we discuss the possible application to the formation of active regions in the sun. Finally, in **Paper VIII** the possibility of additional effects that emerge once the resulting magnetic field becomes strongly nonuniform and terms involving the mean current density introduce new effects.

2. Turbulence and magnetic fields

Big whirls have little whirls
that feed on their velocity,
and little whirls have lesser whirls
and so on to viscosity.

Lewis F. Richardson, 1922

2.1 The basic equations

As all the relevant length and time scales are much larger than the ones associated with collisions and plasma relaxation, we are safe in assuming ourselves in a fluid regime. The main equations used throughout this thesis, namely those of magneto-hydrodynamics (MHD), are the continuity equation (conservation of mass)

$$\partial_t \rho = -\boldsymbol{\nabla}\cdot(\rho \boldsymbol{U}), \tag{2.1}$$

the momentum equation

$$\rho\partial_t \boldsymbol{U} + \rho \boldsymbol{U}\cdot\boldsymbol{\nabla}\boldsymbol{U} = -\boldsymbol{\nabla} p + \boldsymbol{J}\times\boldsymbol{B} + \rho\boldsymbol{g} + \rho\nu\left(\nabla^2\boldsymbol{U} + \tfrac{1}{3}\boldsymbol{\nabla}\boldsymbol{\nabla}\cdot\boldsymbol{U} + \mathsf{S}\cdot\boldsymbol{\nabla}\ln\rho\right), \tag{2.2}$$

with $\mathsf{S}_{ij} = \frac{1}{2}\left(\partial_i U_j + \partial_j U_i\right) - \frac{1}{3}\delta_{ij}\boldsymbol{\nabla}\cdot\boldsymbol{U}$ and the induction equation

$$\partial_t \boldsymbol{B} = \boldsymbol{\nabla}\times(\boldsymbol{U}\times\boldsymbol{B} - \eta\mu_0\boldsymbol{J}), \tag{2.3}$$

where the electric field has been eliminated from the Faraday equation by using Ohm's law, and where η is the magnetic diffusivity. The magnetic field is divergence free. We use a standard notation with density ρ, velocity $\boldsymbol{U}$, gravity $\boldsymbol{g}$, gas pressure p, magnetic field $\boldsymbol{B}$, current density $\boldsymbol{J} = \boldsymbol{\nabla}\times\boldsymbol{B}/\mu_0$, kinematic viscosity ν (assumed constant here). Generally, one also includes the conservation of energy, however, throughout most of this work we replace the energy equation by an isothermality assumption. Note that this also implies the absence of convection, requiring a different source of turbulence, $\boldsymbol{f}$. Working in units where the vacuum magnetic permeability is unity, $\mu_0 = 1$, we can rewrite the momentum equation as

$$\partial_t \boldsymbol{U} = -\frac{1}{\rho}\boldsymbol{\nabla}\cdot\left(p\boldsymbol{I} + \boldsymbol{U}\boldsymbol{U} + \frac{1}{2}B^2\boldsymbol{I} - \boldsymbol{B}\boldsymbol{B}\right) + \boldsymbol{g} + \nu\left(\nabla^2\boldsymbol{U} + \tfrac{1}{3}\boldsymbol{\nabla}\boldsymbol{\nabla}\cdot\boldsymbol{U} + \mathsf{S}\cdot\boldsymbol{\nabla}\ln\rho\right) \tag{2.4}$$

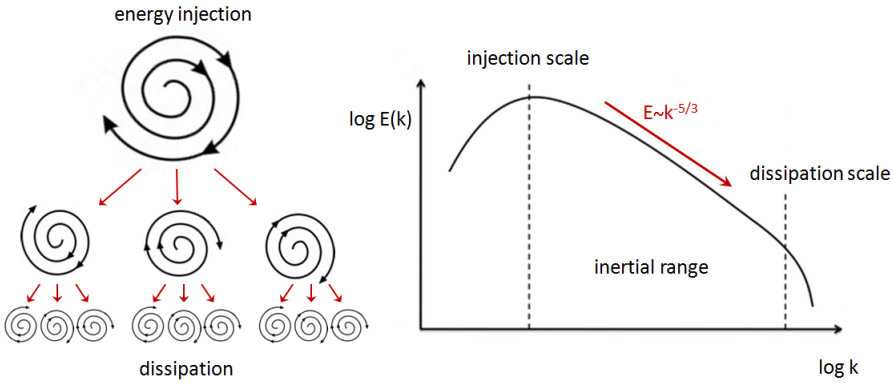

Figure 2.1: Energy cascade for isotropic turbulence, the $-5/3$ scaling of spectral energy E contained in the scale $1/k$ in the inertial range can be found from dimensional analysis (Kolmogorov, 1941) (right). Sketch of self-similar decay of turbulent motions ('eddies') (left).

where $\boldsymbol{f}$ is a volume velocity forcing, and $\boldsymbol{I}$ is the unity tensor. Note that the Lorentz force has been reformulated as the divergence of the Maxwell stress. By adding the latter to the stress tensor $\boldsymbol{UU}$ and the isotropic pressure tensor $p\boldsymbol{I}$, we can define a total pressure tensor $\boldsymbol{\Pi}$

$$\boldsymbol{\Pi} = p\boldsymbol{I} + \boldsymbol{UU} + \frac{1}{2}B^2\boldsymbol{I} - \boldsymbol{BB}. \tag{2.5}$$

It is this tensor which is modeled in Chapter 5.

2.2 Turbulence

2.2.1 Cascade

In a fluid, viscous dissipation of energy occurs on small scales. However, this energy is usually injected on much larger scales, typical energy sources can be divided into: direct mechanical forcing (stirring a cup of tea, supernova explosions in the interstellar medium), boundary layers (flow over a wing) and gradient instabilities (interface between 2 fluids with different velocities).

We need a way to transfer energy from the injection scale to the dissipation scale, this happens through a turbulent cascade. The simplest picture is that of fluid turbulence (Richardson, 1922), where isotropic eddies, break up into smaller ones until dissipation sets in, a schematic illustration is given in figure 2.1. This picture becomes more complicated when there are anisotropies

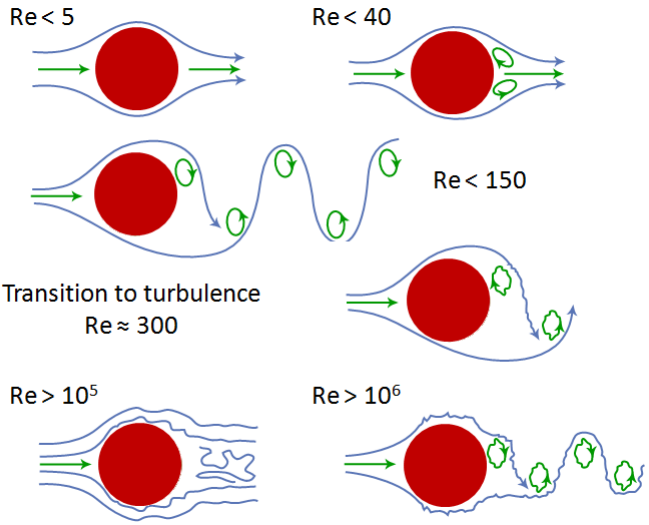

Figure 2.2: Flow around a cylinder for different values of the Reynolds number, from laminar to fully turbulent (Lienhard, 1966).

in the system (like gravity or strong magnetic fields) or when there are multiple dissipation paths (for example a combination of diffusion and excitation of Alfvén waves).

The scale range between injection and dissipation where energy transfer is dominated by a self similar transfer of kinetic energy to smaller scales, is the 'inertial range'. In most astrophysical applications it can be quite large.

2.2.2 Stochasticity

The energy transfer from large scale motions to smaller scales is a non-linear interaction. Due to this non-linearity, the dynamical behaviour of fluids strongly depends on small perturbations, for example caused by initial or boundary conditions (or round off errors in the case of computer simulations). In many circumstances these effects are so pronounced, that statements about the long term evolution of a flow are, in general, true only in a statistical sense.

The relative importance of the non-linear term in the momentum equation with respect to viscous dissipation is estimated by the Reynolds number, $Re = ul/\nu$, where l and u are turbulence associated velocity and length scales. As the Reynolds number increases, a steady flow turns unsteady and eventually becomes turbulent. A very well studied example of such a scenario is given in figure 2.2. A corresponding quantity can be defined for the induction equation: $Re_{\mathrm{M}} \approx ul/\eta$. The ratio of the two, $Pr_{\mathrm{M}} = Re_{\mathrm{M}}/Re = \nu/\eta$ is called the

magnetic Prandtl number.

2.3 Dealing with turbulence

2.3.1 Modelling turbulence

Physical phenomena observed on large spatial and temporal scales can be manifestations of processes happening on much smaller scales, for example turbulent transport across a confining magnetic field. Unfortunately the 'easy' way out, just using brute force, resolving the dynamics on all relevant scales, referred to as 'direct numerical simulations' (DNS), while in itself not really adding any understanding, is also computationally costly and usually, like in the case of the Sun, virtually impossible. To realise global scale simulations, it is necessary to model the effects due to the physics occurring on scales that are not resolved.

Two general formalisms are commonly used: large eddy simulations (LES), where spectral filtering is applied to distinguish between resolved and modelled scales, and mean field theory (in fluid dynamics also known as Reynolds averaged Navier-Stokes or RANS) where the distinction is made between quantities with finite and vanishing averages. While the latter involves more physical input, it also has applicability limitations due to the averaging procedure over broader spatial scales. LES, on the other hand, tend to ignore anisotropies and are aimed at truncating the turbulent cascade to be computationally manageable.

For both methods we should keep in mind that they are models, and as such always have uncertainties and a finite validity domain (as do the fluid equations they are based on). Exploring the boundaries of that domain should be done while carefully evaluating correctness and completeness of the model in comparison with (numerical) experiments.

2.3.2 Mean-field theory

In the mean-field approach we distinguish between averaged ($\overline{F}$) and fluctuating (f) quantities,

$$F = \overline{F} + f. \tag{2.6}$$

Despite the resemblance of equation (2.6) to a perturbation equation, mean-field theory does not make any assumption about the relative strength of the fluctuations. On the other hand the averaging procedure is constrained by the Reynolds averaging rules, requiring that the average of the fluctuating component is zero and that the averaging operator must commute with respect to

summation, derivation and multiplication with an averaged quantity:

$$\overline{f} = 0, \tag{2.7}$$

$$\overline{F+G} = \overline{F} + \overline{G}, \tag{2.8}$$

$$\overline{\partial_s F} = \partial_s \overline{F}, \tag{2.9}$$

$$\overline{\overline{F}G} = \overline{F}\,\overline{G} = \overline{F\overline{G}}. \tag{2.10}$$

While these rules seem natural, in practice they are not obeyed by many averaging procedures. An important exception are averages over periodic coordinate directions. Yet, for example, in spatial or time averaging, errors introduced by violations of the Reynolds rules become negligible if the separation between the averaging scale and the scale over which the mean fields vary is large enough: integrating $F = \overline{F} + f$ over a dimension with length L only returns $\overline{F}$ when variations in f average out to 0 over this scale L and deviations of F over scale L are still small,

$$\frac{1}{L}\int_L F\,\mathrm{d}x = \frac{1}{L}\int_L \overline{F}\,\mathrm{d}x + \frac{1}{L}\int_L f\,\mathrm{d}x \approx \overline{F}, \tag{2.11}$$

if the scale of variation of f, namely $|\boldsymbol{\nabla}\ln f|^{-1}$, is much shorter than the scale of variation of $\overline{F}$, namely $|\boldsymbol{\nabla}\ln\overline{F}|^{-1}$, i.e.,

$$|\boldsymbol{\nabla}\ln f|^{-1} \ll L \ll |\boldsymbol{\nabla}\ln\overline{F}|^{-1}. \tag{2.12}$$

Unfortunately, this limits the applicability of mean-field theory to situations where such a scale separation can be found.

Example: turbulent dynamo

Let us now look at the effect of turbulence on the evolution of a magnetic field from a mean-field perspective. For a setup where the velocity field is a simple shear flow $(0, Sx, 0)$ (the flow direction is orthogonal to its gradient) and the magnetic field is given by $(B_x(z), B_y(z), 0)$, equation (2.3) reduces to

$$\partial_t B_y = B_x S + \eta\nabla^2 B_y, \tag{2.13}$$

$$\partial_t B_x = \eta\nabla^2 B_x. \tag{2.14}$$

It is evident that B_y can be generated by shearing of the B_x component. However, as no source seems available for the latter, the system will eventually just decay on a resistive timescale. This field generation by shear is referred to as the Ω-effect. The reason being that in rotating bodies (i.e. the solar interior), the shear generally corresponds to differential rotation and commonly denoted by Ω.

Let us now include the effects of velocity fluctuations; i.e. we take $\boldsymbol{U} = (0, Sx, 0) + (u_x, u_y, u_z)$, where $\overline{\mathbf{u}} = 0$. After performing an averaging operation according to the rule of Reynolds averages, we split the involved quantities of equation (2.14) into their mean and fluctuating parts. We can now separately consider the evolution of the mean components:

$$\partial_t \overline{B}_y = (\nabla \times \overline{\mathbf{u} \times \mathbf{b}})_y + \overline{B}_x S + \eta \nabla^2 \overline{B}_y, \tag{2.15}$$

$$\partial_t \overline{B}_x = (\nabla \times \overline{\mathbf{u} \times \mathbf{b}})_x + \eta \nabla^2 \overline{B}_x, \tag{2.16}$$

with $\boldsymbol{B} = \overline{\boldsymbol{B}} + \boldsymbol{b}$, where an additional term compared to the total field equations, now emerges. This term is an average that depends on the correlation between magnetic and velocity fluctuations, and is called the mean electro-motive force (EMF).

Rather than computing this term from the evolution equations for the fluctuating quantities, we can close the equations by modelling these fluctuation correlations in terms of mean fields. The simplest assumption one can make is that the EMF depends only on the local value of the mean quantities, and in particular on the local value of the mean magnetic field and its spatial derivatives:

$$(\overline{\mathbf{u} \times \mathbf{b}})_i = \alpha_{ij} \overline{B}_j + \eta_{ijk} \partial_k \overline{B}_j = \overline{\mathcal{E}}_i, \tag{2.17}$$

where the turbulent transport coefficient tensors α and η themselves may depend on mean field quantities. If there is a non-zero α, it is possible to generate a $\overline{B}_x$ starting from a finite field in the y direction. This is the α-effect, described by Steenbeck, Krause, and Rädler (1966). The resulting generation of magnetic energy from kinetic energy is indicated by the term 'dynamo' (see also Moffatt, 1978). Note that in a similar fashion also the fluctuating component of the magnetic field can be amplified by the interaction with turbulent motions, resulting in an increase in magnetic energy even in the absence of a mean field. This phenomenon is referred to as a fluctuation dynamo (Kazantsev, 1968; Kazantsev et al., 1985; Schekochihin et al., 2004; Zeldovich et al., 1990).

In the isotropic case the EMF expression reduces to

$$\overline{\boldsymbol{\mathcal{E}}} = \alpha \overline{\boldsymbol{B}} - \eta_{\mathrm{t}} \overline{\boldsymbol{J}}, \tag{2.18}$$

where η_{t} can be interpreted as a turbulent diffusivity. Later in this work we will approximate the latter by

$$\eta_{\mathrm{t}} = \tfrac{1}{3} u_{\mathrm{rms}} / k_{\mathrm{f}}, \tag{2.19}$$

where $1/k_{\mathrm{f}}$ is the forcing scale and u_{rms} the mean turbulent velocity. This expression is based on the first order smoothing approximation; see also Krause and Rädler (1980).

Dynamos are believed to be responsible for a major fraction of the large-scale magnetic fields observed in the universe (Zeldovich et al., 1983), from galaxies to the field of our own little planet. The need for dynamos is not always obvious. In galaxies, the Ohmic decay times exceed the age of the universe (14 billion years). However, the gas is turbulent (driven by supernova explosions) and the turbulent decay time is only about a hundred million years. Therefore, the field must be supplied by a dynamo. By contrast, in the Earth's core, the Ohmic decay time is only of the order of ten thousand years, so the need for a dynamo is very obvious. In the Sun, the Ohmic decay time is again quite long, so a large scale magnetic field could survive in the radiative interior for long times, but it would be difficult to explain reversals on an 11 year time scale.

2.3.3 Closure models

The turbulent transport coefficients in the case of the dynamo discussed above are an example of a closure model. The coefficients can be obtained from measurements or analytical estimates or they can be calculated from equations for the fluctuation correlations, which eventually will introduce further unknowns (which have to be modelled). These models generally have a certain parameter range for which they are valid. Extrapolation to a different regime is not necessarily possible and should always be compared with measurements (experimental or DNS).

Below I give two examples of closure models for the induction equation as presented in the first two papers. Later on, in the final chapter, we will look at a closure model for the momentum equation in order to describe the change in the Reynolds stress and the fluctuation component of the mean Maxwell stress in the presence of a mean magnetic field.

Kinematic mean-field induction (Paper I)

In the following we look at the measurement of turbulent transport coefficients from direct numerical simulations. A recently developed approach for doing this is the test-field method (Schrinner et al., 2005, 2007). The original method was derived for the kinematic regime, where the flow is unaffected by the magnetic field, and where consequently the induction equation is linear in the magnetic field. The idea is to measure the response of the system to a mean magnetic field by solving numerically the equations for the fluctuations that arise from the interaction between a given 'test-field' $\overline{\boldsymbol{B}}^{(q)}$ and the turbulent motions. Unlike commonly used analytical approaches to solving this equation, we do not omit the terms that are nonlinear in the fluctuations.

If we look at the equation for the fluctuating component of the magnetic field $\boldsymbol{b}^{(q)}$ (obtained by subtracting the terms with a finite average from the induction equation, equation (2.3)) generated by the presence of this test-field

$$\partial_t \boldsymbol{b}^{(q)} = \nabla \times [\overline{\boldsymbol{U}} \times \boldsymbol{b}^{(q)} + \boldsymbol{u} \times \overline{\boldsymbol{B}}^{(q)}] + \eta \nabla^2 \boldsymbol{b}^{(q)} + \nabla \times [\boldsymbol{u} \times \boldsymbol{b}^{(q)} - \overline{\boldsymbol{u} \times \boldsymbol{b}^{(q)}}], \quad (2.20)$$

we find a linear equation in $\boldsymbol{b}^{(q)}$ with coefficients $\overline{\boldsymbol{U}}$ and $\boldsymbol{u}$ taken from an actual flow field). We can then use this quantity to compute the fluctuation correlations $\overline{\boldsymbol{u} \times \boldsymbol{b}^{(q)}}$ as a function of the magnetic field.

In this case the coefficients will depend only on the flow. One can relax the kinematic condition to having the velocity depend on a mean magnetic field. This requires solving the usual induction equation along with the test-field equations. The crucial assumption here is that the magnetic fluctuations are due to tangling of the mean magnetic field and that fluctuation dynamo generated fields (see section 2.3.2) do not produce systematic correlations with the velocity field and consequently equation (2.20) remains linear in $\boldsymbol{b}^{(q)}$. When these conditions are not met, a fully nonlinear test-field method, e.g. that of Rheinhardt and Brandenburg (2010) must be employed. So far, however, the quasi-kinematic method proved sufficient in all cases of practical interest, with the exception of artificially constructed counter examples with magnetic forcing.

In **Paper I** we develop a method to measure the turbulent transport coefficients (the tensors α_{ij} and η_{ij}) in the expression for the EMF, given by equation (2.17), in the case where the turbulence has one preferred direction. The latter could be for example a rotation axis, the orientation of gravity or a strong magnetic field. This axisymmetry reduces the number of possible non-zero coefficients, from $9+27=36$ to 9. For this smaller number of coefficients we can analyse their physical origins (for example their dependence on the presence and strength of rotation) and the contribution of the associated terms to the behaviour of the magnetic field (such as pumping effects, diffusion or field generation). In addition, to study the dependence of these transport coefficients on rotation and gravity, and to compare these results with earlier analytical calculations, we also estimate the effect of scale separation (defined as the ratio of the wavelength of the spatially sinusoidal test fields to the turbulent forcing scale). We find that some coefficients show an extremum at intermediate separation values, which indicates that at these scale ratios the coefficients can no longer be defined locally and one needs to define averages in terms of convolutions; see Brandenburg et al. (2008); Rheinhardt and Brandenburg (2012).

Non-linear mean-field induction (Paper II)

In plasma experiments, contrary to most astrophysical environments, the dynamics are often dominated by the magnetic fields (applied for confinement purposes). Therefore, in this case the induction equation is strongly nonlinear.

In **Paper II** we address the question to what extent the astrophysical EMF model can be applied in this context. We base our setup on the reversed field pinch (RFP). In this experiment a current is driven in a toroidal plasma through a transformer with the plasma as the passive circuit. This plasma current then induces (poloidal) magnetic fields winding around the plasma. The combination of this induced field and an externally applied toroidal field (current rings around the vessel), of approximately the same magnitude, is then used to confine the plasma. The RFP is mostly used to study MHD instabilities in magnetically confined plasmas (Ortolani and Schnack, 1993), as, due to these instabilities, its energy confinement is too poor to be considered as a fusion reactor. The motivation for this setup choice was the importance of the EMF in terms of stability and earlier work on the α–effect in plasma experiments by Ji and Prager (2002).

We know from Pouquet et al. (1976) that we can approximate

$$\alpha \approx -\frac{\tau}{3}\overline{\boldsymbol{u}\cdot\boldsymbol{\omega}}+\frac{\tau}{3}\overline{\boldsymbol{j}\cdot\boldsymbol{b}}/\overline{\rho}=\alpha_{\mathrm{K}}+\alpha_{\mathrm{M}}, \tag{2.21}$$

with τ the turbulent correlation time. Here, we are mostly interested in the second term. For weakly inhomogeneous turbulence we can relate the current helicity (in the fluctuations) to the magnetic helicity

$$\overline{\boldsymbol{j}\cdot\boldsymbol{b}}\approx k_f^2\overline{\boldsymbol{a}\cdot\boldsymbol{b}}. \tag{2.22}$$

Hence, to understand how α_{M} behaves, we have to look at the time evolution of the magnetic helicity in the fluctuations,

$$\partial_t\alpha_{\mathrm{M}}\approx\frac{\tau k_f^2}{3\overline{\rho}}\partial_t\overline{\boldsymbol{a}\cdot\boldsymbol{b}}=\frac{\tau k_f^2}{3\overline{\rho}}\left(-2\overline{\boldsymbol{\mathcal{E}}}\cdot\overline{\boldsymbol{B}}-2\eta\overline{\boldsymbol{j}\cdot\boldsymbol{b}}-\boldsymbol{\nabla}\cdot\overline{\boldsymbol{\mathcal{F}}}\right). \tag{2.23}$$

Here, $\overline{\boldsymbol{\mathcal{F}}}$ is the mean flux of magnetic helicity in the fluctuations. An equation of this form, was first proposed by Kleeorin and Ruzmaikin (1982). The role of the magnetic helicity fluxes was understood later (see also Blackman and Field, 2000; Brandenburg and Subramanian, 2005; Kleeorin et al., 2000). In our paper we solve the equation above along with the mean induction equation for a cylindrical geometry where the variables depend only on radius.

As this is a very simplified setup, we can reproduce only a few features of the actual experiment. We find a decay of the field which, above a minimal value, is slower than would be anticipated by just taking into account the

diffusive effect of turbulence: turbulent diffusion and field generation approximately balance.

The second focus of the paper revolves around the reproduction of the peculiar RFP magnetic field profile, which we can approximate by Bessel functions $B_z \approx J_0(kr)$ and $B_\phi \approx J_1(kr)$, where B_z reverses sign at an intermediate radius r with $kr \approx 2.40$ and a coefficient k.

We find that this reversal occurs to a reasonable degree only when we have helicity fluxes within the domain. An even stronger effect occurs when we have a finite $\alpha_{\rm K}$. However, as our setup is only one dimensional and the turbulence assumed to be isotropic, a more advanced study would be needed to confirm and perhaps improve these results.

3. Numerical simulations

"I don't actually think," he said, gloomily,
"that I want to tell the Archchancellor that this machine stops working if we take its fluffy teddy bear away.
I just don't think I want to live in that kind of world."
"Er," said Mad Drongo, "you could always, you know, sort of say it needs to work with the FTB enabled...?"

Sir Terry Pratchett, 1997

3.1 Solving PDEs numerically

This section mainly focuses on the methods applied in the PENCIL CODE, which was used in the simulations presented in this thesis.

3.1.1 Spatial derivatives: 'finite difference code'

In our numerical approach we solve partial differential equations through a finite difference scheme. This means that we compute derivatives through polynomial interpolation on a grid. In this sense, a high order code means we use a higher order polynomial, and a larger number of points. When we say that the PENCIL CODE is 6th order in space, using a central finite difference scheme, we mean that we use 3 points on either side of a given point to compute its derivative. This has implications for boundaries and parallelisation where one will need, respectively, 3 ghost points outside the domain or 3 points from the neighbouring processor. For an overview of other approaches to the numerical calculation of spatial derivatives, see Peiró and Sherwin (2005).

3.1.2 Time evolution

The Runge Kutta method (Press et al., 1992) is a reasonably simple yet robust integration scheme and quite commonly used in fluid codes. The method relies on an intermediate step to cancel out lower order corrections in terms of Taylor expansions, as an example I give here the general third order scheme for a

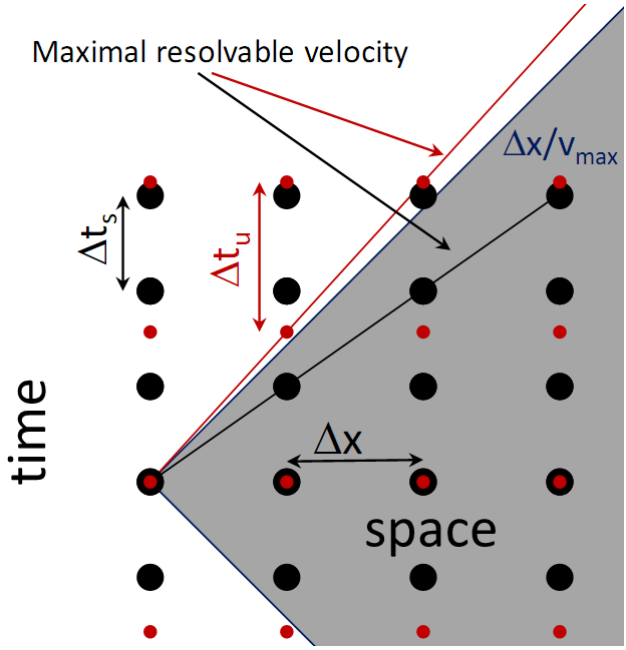

Figure 3.1: Illustration of the CFL condition in analogy with the light cone concept. For the black grid the latter is met and all physical communication (white area) can be resolved, in the red grid the time step is too large, setting a numerical upper boundary to propagation of information.

dependent variable y:

$$k_1 = f(t_n, y_n), \tag{3.1}$$
$$k_2 = f(t_n + \alpha_2 \Delta t, y_n + \beta_{12} k_1 \Delta t), \tag{3.2}$$
$$k_3 = f(t_n + \alpha_3 \Delta t, y_n + (\beta_{13} k_1 + \beta_{23} k_2) \Delta t), \tag{3.3}$$
$$y_{n+1} = y_n + \Delta t (b_1 k_1 + b_2 k_2 + b_3 k_3) + O(\Delta t^4). \tag{3.4}$$

The coefficients are constrained by $\sum_i \beta_{ij} = \alpha_j$ and $\sum_i b_i = 1$, and 3 coupling equations to make the lower order terms drop out. The remaining degrees of freedom can be used to for example minimise data storage (Williamson, 1980).

From figure 3.1 we see that if the time step is chosen too large, the maximal resolvable propagation speed is less than the physical one, therefore the step size is constrained by

$$\Delta t < \Delta_x / v_{max}. \tag{3.5}$$

This is also known as the CFL condition (Courant, Friedrichs, and Lewy, 1928); it is a necessary (but not sufficient) condition for stability. Note that

from this requirement it follows that increasing the resolution of a simulation will decrease the length of the time step.

3.2 Numerical 'experiment'

To some people the word 'experiment' sounds strange in a simulation context, after all we are solving a set of equations, which are by definition models.

Indeed, a first concern is the question whether the model is valid under the tested conditions. For example, the fluid equations are not general enough to take into account effects caused by non-Maxwellian velocity distributions, like Landau damping, and will give unrealistic results when such phenomena do occur. On the other hand including more physics will require more, perhaps unnecessary, computations: anything you add you have to solve and resolve. It is therefore important to know approximately what to expect and to test assumptions you make. In short, it is time to start thinking 'laboratory' when the physics gets too complex or is fairly unknown.

A second major issue is one of resolution. For example when calculating the behaviour of turbulent flows in direct numerical simulations, i.e. without any subgrid scale modelling, it is necessary to resolve all the energy containing scales, from the domain size that you are interested in, over the turbulent injection scale, down to the scale where energy is dissipated. This makes it hard to achieve high Reynolds numbers (which scales with the ratio between the turbulent injection and the dissipation scale) in simulations. Resolution issues are not limited to turbulence. Also, for example, dealing with shocks, resonance related physics and high curvature surfaces, are very resolution demanding.

While the question 'is it real?' is of course an important one, in return there are also several advantages over laboratory experiments, which in a sense stem from the distance to reality. The computer scientist is omnipresent: diagnostics can measure any variable in any location. He is omnipotent: initial and boundary conditions are perfectly controllable, even physical laws can be altered (to verify the effect of different terms, enforcing isothermality rather than building a complex cooling mechanism), there is no restriction to existing material properties (and no safety issues due to for example explosion hazards in case of water contact).

3.3 PENCIL CODE: open, modular, parallel

The PENCIL CODE is an open code: it is freely available and adaptable, daily testing ensures that those adaptations are beneficial. In combination with its very modular structure, equations can be solved or omitted depending on the

problem, this has lead to a very broad spectrum of applications. Originally addressing astrophysical MHD, it has branched out into the domain of planet formation with particles (Johansen et al., 2007), radiative transfer (Heinemann et al., 2006), as well as chemistry and combustion physics (Babkovskaia et al., 2011). More extensive information can be found in the manual.

To tackle current day questions, large scale computations are required. The PENCIL CODE is a parallel code and has shown approximately linear scaling for up to 4096 processors.

3.4 Runs and their analysis

This section is mostly to illustrate how the more general principles, described above, affect our simulations.

What sets our resolution and timestep? Both in DNS and mean-field simulations we are limited by the density contrast (in our simulations $\rho_{max}/\rho_{min} \approx 500 - 1000$): too low resolution would cause the density gradient to become under-resolved. In DNS there are two more restrictions from the turbulence, the combination of which sets severe restrictions on the resolvable Reynolds number. Our largest scale is set by the turbulent energy injection scale: in order to be able to have sufficient scale separation, the ratio of the domain size to the turbulence forcing scale is chosen to be between 15 and 30 for most of the runs. The smallest scale we need to resolve is set by dissipation. The ratio between inertial scale (1/15 to 1/30 of the box size) and dissipation scale (say 1/256 for a simulation with 512^3 mesh points) restricts the largest value of $Re_{\rm M}$ to be between 10 and 20 (for this setup).

Note that in a convection setup the stratification is locally even stronger. At the same time turbulent scales are height dependent, such that the turbulent scales near the top are much smaller than deeper down in the domain. Consequently the associated Reynolds number will be quite low, even for a very high resolution.

How strongly do we alter reality? We have made a strong simplification by considering a stably stratified medium with random forcing rather than studying the convective setup. Doing this we also lost the possibility to generate a magnetic field through a mean-field dynamo; hence we imposed a magnetic field, with a simple geometry. These simplifications were made both to limit the numerical cost and to isolate and first understand a minimal problem, with the intention to incorporate complications one step at a time. The implications of these assumptions are addressed in section 5.5.

For the magnetic field we have perfect conductor boundary conditions, which seems reasonable given the high plasma conductivity, and for velocity stress free conditions at top and bottom, making them material surfaces. A

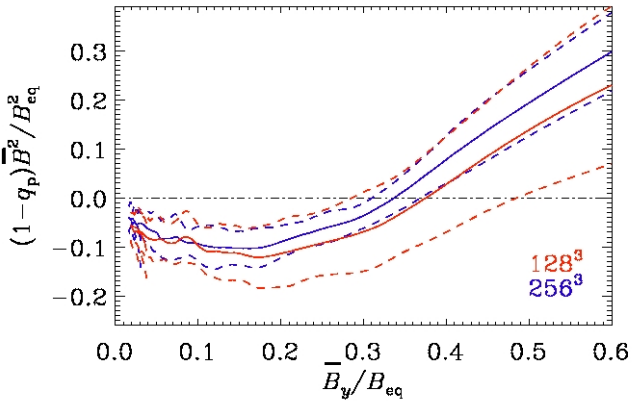

Figure 3.2: Comparison of DNS calculation of the negative effective magnetic pressure effect for the same setup at two different resolutions, showing the 256^3 curve well within the error bars (dashed lines) of the 128^3 result. Adapted from figure 7 of **Paper III**.

comparison of different resolutions in figure 3.2 indicate that resolution corrections are well within the error margins.

In **Paper VIII** it was only possible to give a qualitative indication of the effect of currents on the instability as the calculation of higher order derivatives, currents are the second order spatial derivative of the calculated vector potential, in a turbulent environment comes with rather large error bars.

To finalise this chapter some numbers to give an idea of the size of the calculations. The extraction of the effective pressure curve from DNS requires two separate simulations per setup: one with and one without an imposed magnetic field. This brings the typical computation cost to easily 20000 CPU hours for a 256^3 simulation. Two-dimensional mean field calculations, 256^2, only require about 30 CPU hours.

4. Magnetic fields on the solar surface

Sunspots are the classic example of long standing ignorance,
well known to observation for centuries,
possessing fascinating internal fine structure,
and still not understood from the basic laws of physics.

E.N. Parker, 2009

4.1 Sunspots as a part of the solar dynamo

The current standard idea about sunspot formation stems from a paper by Parker (1955), where he suggests the buoyant rise of magnetic flux tubes to the surface. As the magnetic field contributes to the pressure inside a magnetic flux tube we see from horizontal pressure balance that the gas pressure and thus the density (ρ_i) inside must be lower than outside (ρ_e) (assuming thermal adjustment is fast).

$$\rho_\mathrm{i} RT + B^2/2 = \rho_\mathrm{e} RT. \tag{4.1}$$

As the density is lower inside the tube, it becomes buoyant and rises. The rising flux tube expands because the pressure higher up is lower than the total pressure inside a tube of unchanged thickness. Given that the field is frozen in, this density reduction also causes a dilution of the magnetic field. As the density contrast between the top and bottom of the convection zone is approximately 4 orders of magnitude (not counting the upper 6Mm) and sunspots have kgauss fields, this would require very strong initial fields at the bottom. To rise somewhat coherently, in a turbulent medium like the convection zone, the flux tube needs to be twisted (Parker, 1979). This was also verified in simulations by Longcope et al. (1996) and Fan et al. (2003). Note, however, that there is also an upper limit to the amount of twist, set by the onset of kink instabilities (Linton et al., 1996).

This raises questions where these tubes come from, how strong they should be to match surface observations and to remain intact, and how they form in that environment to match these conditions. In the picture sketched by Babcock (1961), see figure 4.1, flux tubes are formed from a toroidal magnetic field in the convection zone. This field in turn would be the result of shearing

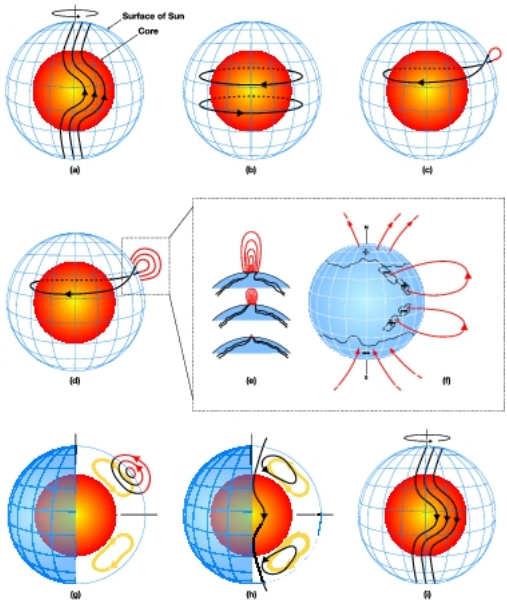

Figure 4.1: Flux transport model for the solar dynamo cycle, i.e. similar to the mechanism proposed by Babcock (1961), but with the toroidal field confined near the tachocline

of the global (poloidal) dipole field by differential rotation. As a result of the Coriolis force, flux tubes twist as they rise to the surface, generating a poloidal field component to reinforce the dipole.

Given that magnetic fields above 100 gauss would rise due to magnetic buoyancy, Parker (1975) argued that it would be hard to keep fields long enough for them to be amplified by shearing. Storage in the stably stratified region below would be feasible for very long times, but there needs to be some interaction with the convection zone for the dynamo to operate. This restricts the location of such a toroidal field to a narrow region at the base of or just below the convection zone.

Choudhuri and Gilman (1987) calculated that, if flux tubes are to rise from the base of the convection zone to near equator latitudes, their field strength should be on the order of 10^5 gauss. For weaker fields the flux tubes would be deflected polewards by the Coriolis force: the interaction of radial rise and rotation generates a toroidal motion, which in turn is directed towards the axis by the rotation, giving the tube a poleward velocity. It is then assumed that either a homogeneous or a fibril magnetic field of this strength is stored in the overshoot layer. Ruzmaikin (1998) proposed that the stored field need not be that high, as the 10^5 gauss threshold value, in this case more thought of as a minimal survival field strength, can also be reached by the interaction of a

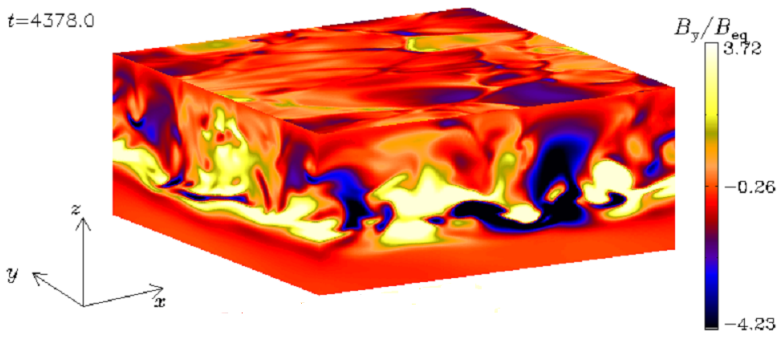

Figure 4.2: Rising magnetic structures in convective simulations by Guerrero and Käpylä (2011).

weaker mean field (10^4 gauss) and a fluctuating field with a high energy tail in its distribution function.

4.2 Assumptions in the standard sunspot model

The question of the formation of flux tubes has yet to be answered. Several mechanisms have been proposed to break magnetic fields free from a magnetic storage layer. But until now none has been able to produce strong (about 100 times the equipartition field) twisted thin flux tubes. A recent result in this context are the convection simulations by Guerrero and Käpylä (2011). These show the formation of large scale elongated field structures from a shear layer, twisted as a result of Kelvin-Helmholtz instabilities, and their rise to the surface. However, upon arrival these magnetic structures are strongly deformed and expanded even though the turbulence and density contrast are still well below solar values.

The pressure balance in equation (4.1) does not take into account the presence of inhomogeneous turbulent convection. It has been shown in simulations that the latter strongly affects the transport of magnetic fields. Starting from respectively a random field distribution and a thin magnetic layer, both Nordlund et al. (1992) and Tobias et al. (1998) found strong downward pumping of the magnetic fields. On the other hand, Guerrero and Käpylä (2011) measured in their simulations, using the test-field method, the downward pumping velocity to be only about half the buoyant rise velocity, resulting in a net upward transport of magnetic field.

A number of near surface simulations have yielded quite good agreement with observations using a flux tube as either boundary or initial conditions, see for example figure 4.3. However, the acceptable realisation at the surface

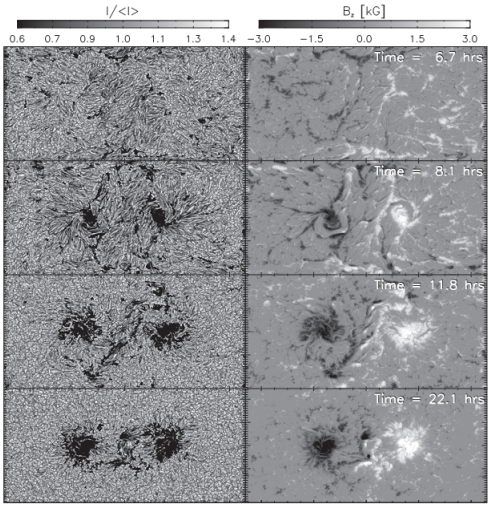

Figure 4.3: Emergence of a sunspot, simulated by Cheung et al. (2010).

does not provide sufficient justification for the magnetic configuration assumed deeper down as a unique solution.

4.3 Incompleteness in the standard sunspot model

Several observed properties of solar surface fields are not correctly reproduced by the rising flux tube paradigm. It has long been known that bipolar structures are systematically tilted with respect to the rotation direction (Joy's law). Calculations in the thin flux tube approximation by D'Silva and Choudhuri (1993) show that the action of the Coriolis force can give emerging tubes such a tilt. However, recent observational analyses by Kosovichev and Stenflo (2008) as well as Stenflo and Kosovichev (2012) have shown that actually this tilt is random upon emergence and then relaxes to a certain angle in a few hours, with a non-negligible fraction of bipolar regions violating Hale's polarity law. They also do not find the correlation between the tilt and the magnetic flux in a spot which would be expected for rising flux tubes. Weber et al. (2012) attribute these differences to convection, which was not present in the earlier model.

Sunspots have a higher azimuthal velocity than the quiet solar surface (Balthasar et al., 1986), coinciding with rotational velocities found in the near-surface shear layer (Thompson et al., 2003) at a depth of about 35 Mm. It is unclear why a rising tube would adopt this velocity.

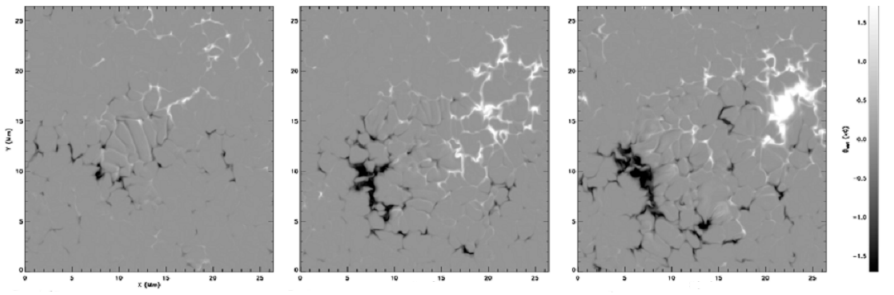

Figure 4.4: DNS showing the emergence of a sunspot as the result of the interaction of turbulent convection and a shallow uniform horizontal field layer (Stein and Nordlund, 2012)

4.4 Alternative suggestions

4.4.1 Convection zone dynamo

Abandoning the idea of a tachoclinic toroidal field would require a dynamo to operate in the convection zone, possibly with an important role for the near surface shear layer (Brandenburg, 2005). The main argument behind the tachocline assumption is that fields should be stored long enough to be amplified by shear, i.e. not buoyantly transported upward and not destroyed by turbulent convection. However, as mentioned earlier, buoyant rise is reduced by downward pumping and their exact balance is unclear.

The typical turbulent time scale, on the order of several days (at 35 Mm depth), is short, but sufficient for amplification purposes. This short scale compared to the cycle length is one of the main arguments against a convection zone dynamo.

Keeping only in mind the picture of turbulent diffusion, it is indeed hard to imagine that these amplified fields can survive in a turbulent environment. However, turbulence is also a source for instabilities that can overcome this turbulent decay.

4.4.2 Sunspots without rising flux tubes

There are now several simulation results indicating possible structure formation near the surface, without assuming rising flux tubes.

Recently, Stein and Nordlund (2012) showed in numerical simulations the formation of rather realistic looking bipolar regions from a uniform horizontal field layer in a convective setup; see figure 4.4. These are the result of the interplay between magnetic buoyancy and advection by convective motions. The exact mechanism responsible for concentrating the rising fields into the

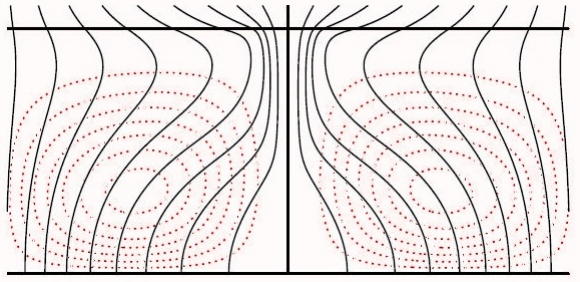

Figure 4.5: Mean field simulation of magnetic structure formation at the surface as a result of magnetically quenched heat transport (Kitchatinov and Mazur, 2000), with magnetic field lines in black, velocity in red.

observed structures remains to be further explored. The lower domain boundary (and the horizontal field layer) in these simulations is located at a depth of about 20 Mm.

In mean-field simulations Kitchatinov and Mazur (2000) find magnetic field concentrations near the surface when turbulent heat transport is magnetically quenched; see figure 4.5. As radiative losses can no longer be compensated by the reduced heat flow, the plasma cools down and, in a compressional downflow, enhances the magnetic field. Smaller scale surface magnetic field concentration, possibly related to, for example, pore formation, are amplification in vortical downdrafts (Kitiashvili et al., 2010) and convective collapse (Spruit, 1976). An other mechanism, originally proposed by Kleeorin et al. (1989) predicts structure formation as the result of suppression of the turbulent pressure by a mean magnetic field. The coefficients in its mean-field description were first analytically estimated in Kleeorin et al. (1990), using the spectral tau approach, and later, in different approximations, in Kleeorin and Rogachevskii (1994); Rogachevskii and Kleeorin (2007). This mechanism is the subject of the next chapter.

5. Turbulent stress and magnetic fields

Eppur si muove.

G. Galilei, 1633

5.1 Effective magnetic pressure

As pointed out earlier, in the mean field formalism we would like to model turbulent correlations in terms of mean fields and their gradients. This means that the mean turbulent stress tensors $\overline{u_i u_j}$, the 'Reynolds stress', and $\delta_{ij}\overline{b^2}/2 - \overline{b_i b_j}$, the contribution of fluctuations to the mean Maxwell stress, can be modelled as a function of the mean magnetic field $\overline{\boldsymbol{B}}$ and its derivative, as well as the derivative of the mean velocity field $\overline{\boldsymbol{U}}$.

In the following we study the effect of a magnetic field on the turbulent stresses and its impact on the total pressure tensor, defined in equation (2.4) as the sum of gas and magnetic pressure. The turbulent component of this tensor can be written as

$$\overline{\Pi}^B_{ij} = \overline{\rho u_i u_j} + \frac{\overline{b^2}}{2}\delta_{ij} - \overline{b_i b_j}. \tag{5.1}$$

Like before, units are defined such that $\mu_0 = 1$, the superscript B refers to the presence of a magnetic field. For isotropic turbulence we can define the turbulent pressure $P_{\rm turb}$ as the trace of this tensor, we find that

$$P_{\rm turb} = \frac{\overline{\rho u^2}}{3} + \frac{\overline{b^2}}{6}. \tag{5.2}$$

Taking into account the fact that turbulent energy is approximately conserved in the presence of uniform weak magnetic fields (Brandenburg et al., 2010):

$$E_{turb} = \frac{\overline{\rho u^2}}{2} + \frac{\overline{b^2}}{2} \approx \text{const}, \tag{5.3}$$

we can see that an increase of magnetic fluctuations (conversion of turbulent kinetic energy into turbulent magnetic energy) reduces the turbulent pressure:

$$P_{\rm turb} \approx \frac{2}{3}E_{\rm turb} - \frac{\overline{b^2}}{6}\Delta P_{\rm turb} \approx -\frac{1}{3}\Delta E^M_{\rm turb}. \tag{5.4}$$

These magnetic fluctuations can be generated by a fluctuation dynamo or by tangling a mean magnetic field: as the fluid motions drag along the field, turbulent motions generate magnetic fluctuations. This raises the question if it is possible to reduce the total pressure by adding a mean magnetic field. We define the 'effective magnetic pressure tensor' P_{ij}^M as this difference:

$$P_{ij}^M = \underbrace{\frac{\overline{B}^2}{2}\delta_{ij} - \overline{B}_i\overline{B}_j}_{\text{direct effect}} + \underbrace{\overline{\Pi}_{ij}^B - \overline{\Pi}_{ij}^0}_{\text{turbulence}} = \frac{\overline{B}^2}{2}\delta_{ij} - \overline{B}_i\overline{B}_j + \Delta\overline{\Pi}_{ij}^B \tag{5.5}$$

From the latter we can define an effective magnetic pressure perpendicular to the magnetic field, which from now on we define to be along the y direction. In that case we have

$$P_{\text{eff}}^M = \frac{B^2}{2} + \frac{1}{2}\left(\Delta\overline{\Pi}_{xx}^B + \Delta\overline{\Pi}_{zz}^B\right) \tag{5.6}$$

5.2 Experiment and model

The model describing $\Delta\overline{\Pi}_{ij}^B$, 'the effective turbulent magnetic pressure tensor', includes a number of simplifications related to the symmetries in the setup used for most of our numerical experiments. Therefore we take a quick look at this setup before continuing.

The initial configuration is that of an isothermally stratified medium with an imposed uniform magnetic field B_{0y} perpendicular to the direction of gravity g_z. This means that the system is stable to convection. Turbulence is instead generated through random forcing with plane waves. In most cases this forcing is non-helical, which implies that there is no α effect and there is no mean-field dynamo.

We would like to model the change in the turbulent pressure tensor in terms of the mean field. We know that this tensor is symmetric and invariant under inversion of the sign of $\boldsymbol{B}$. A first order model would be a linear combination of tensors constructed from mean vector quantities $\boldsymbol{g}$, $\boldsymbol{B}$, $\boldsymbol{U}$ and their derivatives. Note that $\boldsymbol{B}$ is a pseudo-vector (not invariant under parity inversion). In our setup, in the absence of structure formation, the vectors above are constant and the mean velocity is zero, leaving only $\boldsymbol{g}$ and $\boldsymbol{B}$ as building blocks. Furthermore, the coefficient for a pseudo-tensor should be related to pseudo-scalar fluctuation correlations. In this setup cross-helicity, $\overline{\boldsymbol{u}\cdot\boldsymbol{b}}$, is the only such correlation, however, without source (as $\boldsymbol{g}$ is perpendicular to $\boldsymbol{B}$) it is zero and thus $g_iB_j + g_jB_i$ terms drop out. This leaves us with g_ig_j, B_iB_j as well as $\boldsymbol{g}^2\delta_{ij}$

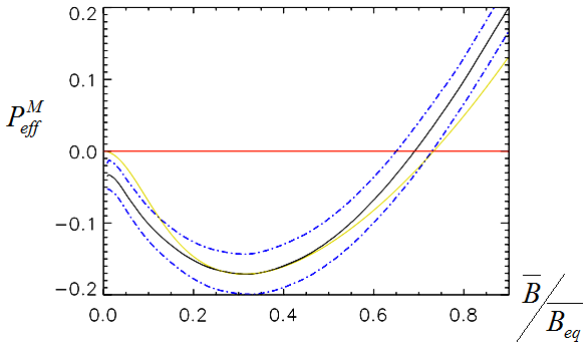

Figure 5.1: Effective magnetic pressure perpendicular to the magnetic field, normalised by equipartition pressure, as a function of the the mean magnetic field, normalised by equipartition field ($R_{\rm m} = 18$, $Pr_{\rm m} = 0.5$). The dashed blue lines indicate error bars, the yellow line is the corresponding fit from equation (5.8).

and $\boldsymbol{B}^2\delta_{ij}$. We can now model the pressure difference as

$$\Delta\overline{\Pi}_{ij}^{B} = -q_p\frac{\overline{B}^2}{2}\delta_{ij} + q_s\overline{B}_i\overline{B}_j + q_g\frac{g_ig_j}{\boldsymbol{g}^2}\overline{B}^2. \tag{5.7}$$

where we subsumed all the isotropic contributions into $q_p\overline{B}^2\delta_{ij}$. Also, as in the absence of a mean magnetic field the difference should become zero, we extracted an explicit $\boldsymbol{B}^2$ dependence from the coefficients. The coefficients can depend on the turbulence (Reynolds number, Prandtl number) as well as $\boldsymbol{g}$ and $\overline{B}^2$. This model becomes less complete as a mean velocity field and mean currents develop in the simulation. This is addressed in **Paper VIII**; see also section 5.4.5.

5.3 Negative effective magnetic pressure (Papers III, IV, VI)

The existence of a reduction of the total turbulent pressure perpendicular to the field ($-\Delta\overline{\Pi}_{xx}^{B} > \overline{\boldsymbol{B}}^2/2$) was demonstrated numerically by Brandenburg et al. (2010) for non-stratified forced turbulence and in **Paper III** for the stratified case, see also figure 5.1, and Käpylä et al. (2012), who observe its presence in convective simulations.

We find that q_s, the reduction of magnetic tension, and q_g, the anisotropy correction due to gravity, are relatively small in the parameter regime that we are studying. In this simple model the q_s term is the only one counteracting the

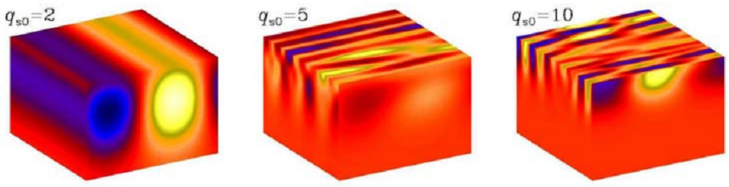

Figure 5.2: When, in mean-field simulations, q_s is small, the mean magnetic field $\overline{B}_y$ does not vary along the direction of the imposed field, adapted from **Paper IV**.

mean field pressure along the field and thus the only one able to affect the geometry in this direction. This was also demonstrated in mean field simulations in **Paper IV**; see figure 5.2. The smallness of this coefficient results in and is confirmed by the observation of the independence of the found solutions on the coordinate along the field. Furthermore, this knowledge allows us to average along the direction of the field to obtain mean fields from DNS, and so in mean field simulations we can limit ourselves to a two-dimensional setup, perpendicular to the field.

The q_p coefficient is a function of the ratio of the magnetic field strength to the equipartition field (indicated by β, not to be confused with its plasma physics namesake, which is the ratio of the gas pressure to the magnetic pressure), the dependency is a function of the magnetic Reynolds and Prandtl numbers. We proposed a phenomenological fit, based on the DNS results:

$$q_p = \frac{q_{p0}\beta_p^2}{\beta_p^2 + \beta^2} \tag{5.8}$$

For large Reynolds numbers the fit parameters seem to converge to a finite value **(Paper VI)**, although the spread in the data as well as the errors of the fits are relatively large. An increase in Prandtl number seems to decrease the pressure reduction. This may be related to the production of magnetic fluctuations even in the absence of a mean field, through a fluctuation dynamo.

5.4 Negative effective magnetic pressure instability

5.4.1 Observation in direct simulations (Papers V & VI)

While not chronological, it is perhaps best to start with the observation of a large-scale instability in direct numerical simulations as a result of the pressure reduction by a mean field. In the linear stage, where the original field configuration is not significantly modified by the instability, we see the exponential growth of magnetic structures along the direction of the imposed field

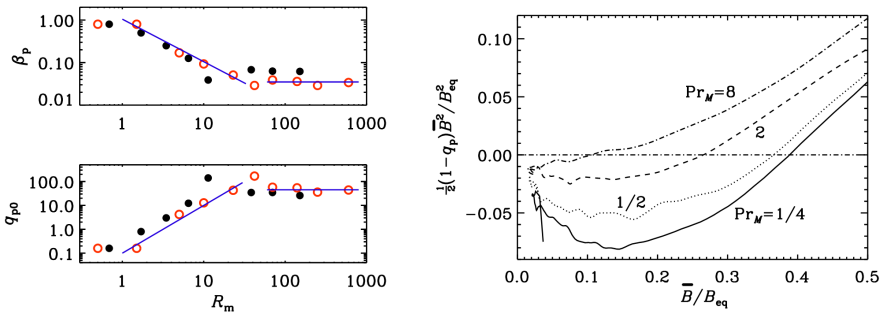

Figure 5.3: Dependency of (normalised) effective magnetic pressure on magnetic Prandtl number and estimate of fitting coefficients for a range of values for the magnetic Reynolds number.

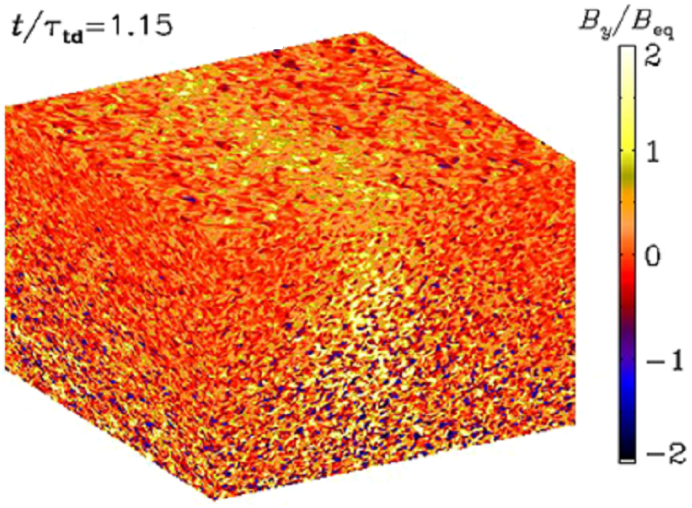

Figure 5.4: Observation of NEMPI in DNS without averaging; the horizontal magnetic field normalised to the equipartition field in the middle of the box, taken from **Paper VI**.

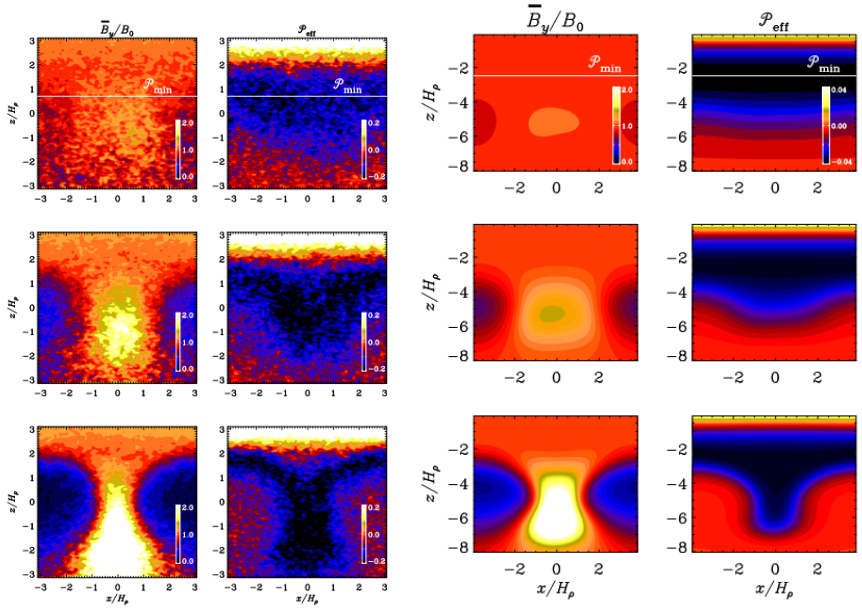

Figure 5.5: Left: Time evolution of the mean (y-averaged) magnetic field and effective magnetic pressure in direct numerical simulations. Right: Time evolution of the magnetic field and effective magnetic pressure in mean-field simulations. Taken from **Paper VII**.

on scales that are large compared to the forcing scale, shown without averaging in figure 5.4 and after taking the average along the field in figure 5.5 (left).

Key to these observations were, on one hand, the conclusion from mean field simulations that it was meaningful to average along the direction of the field and, on the other hand, an increase of scale separation (which reduces turbulent diffusion as $\eta_t \approx u_{\rm rms}/3k_f$) compared to the initial simulations where we did find a turbulent pressure reduction, but no instability.

5.4.2 Reproduction of DNS results in mean-field simulations (Paper VII)

In figure 5.5 (right) we see that the results from two-dimensional mean field models, where we only take the q_p term of the model into account, reproduce the structures found in DNS very well. This agreement shows that the mean-field approach is justified and that our model is quite reasonable for the current setup.

Since these calculations are computationally much cheaper than the direct simulations, they were used for further exploring the behaviour of the instability as a function of different simulation parameters. The results of this search

can be found in **Paper IV**.

5.4.3 Linear instability

When we are below the effective magnetic pressure minimum $\beta_{\min}$, a local increase of the magnetic field causes a decrease of the pressure. This pressure difference with the environment is then compensated by inflows. These drag along magnetic field, which is approximately frozen into the fluid, thus enhancing the initial field perturbation. From this argument it is clear that the maximal field strength that can be reached by this instability is limited to a fraction β_{min} of the equipartition field. Note that, conversely, a local field reduction will result in buoyancy.

If we now add stratification to the picture, we get, on the one hand, an upward negative gradient in effective pressure (the imposed field is constant but density decreases with z) and, on the other hand, a density increase associated with inflows. The balance of these was calculated in a linear stability analysis of the mean field model (without dissipation); for detail see the appendix of **Paper V**. While inflows are expected to be strongest near the location with the strongest vertical effective magnetic pressure gradient, the structures form a bit below that point, which agrees with the observations in the DNS.

A linear stability analysis predicts with reasonable accuracy both the location, see figure 5.6, and growth rate of the instability. The calculated growth rate λ was found to approximately obey the following relation

$$\lambda^2 \approx \frac{C_A^2}{H_\rho^2}\left(1 - q_p - \frac{\partial q_p}{\partial \beta^2}\beta^2\right) - k^2\eta_{\mathrm{t}}, \tag{5.9}$$

with C_A the Alfvén speed and H_ρ the density scale height, omitted in the analysis, the diffusion term was added manually. This result agrees well with the values and trends we found in our mean-field parameter search and is of the same order of magnitude as the DNS measurements.

Taking the derivative of the growth rate above with respect to $\overline{B}$ we find an expression for the value of β associated with the height of the instability, independent of the imposed magnetic field. Hence the only effect of varying the magnitude of the imposed field in the linear stage is a change of the physical height where the instability starts. The growth rate is independent of the mean magnetic field as long as the predicted instability height falls well within the simulation domain. This result was also confirmed in DNS; see figure 5.7.

5.4.4 Nonlinear evolution

At later times, we see that the imposed field gets depleted as the formed structure grows, both in terms of field and density, although the latter is only a

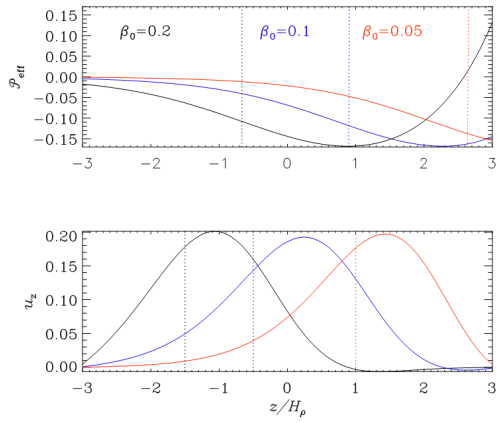

Figure 5.6: Above: fitted effective magnetic pressure curves with indication of the strongest negative gradient in effective magnetic pressure. Below: location of the growing structures (DNS) and eigenmode of the linear instability analysis for the same parameters. Adapted from **Paper VII**.

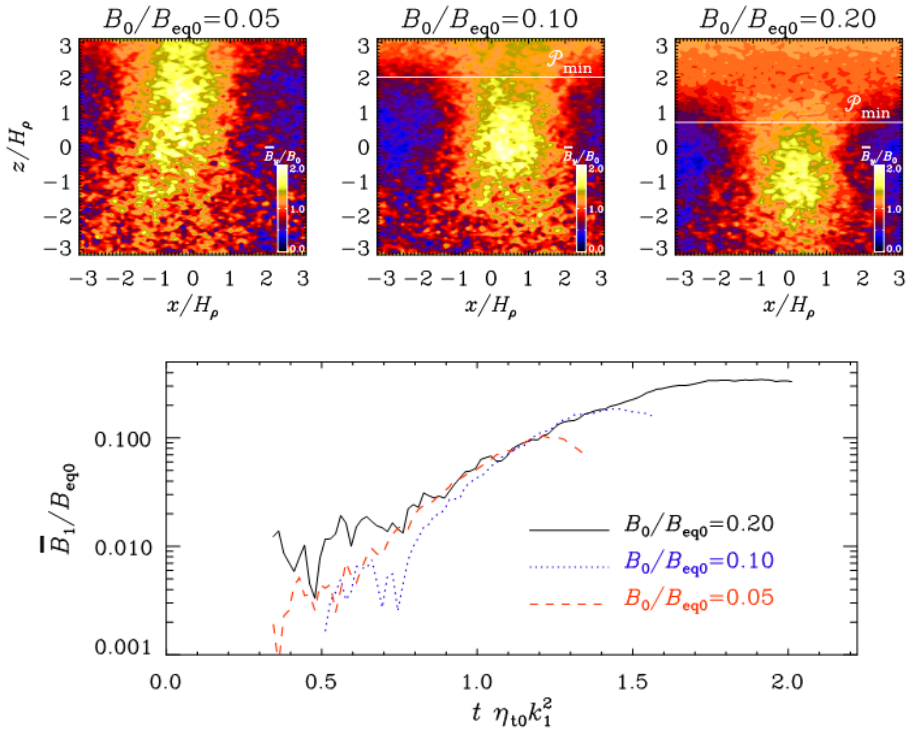

Figure 5.7: Effect of imposed field strength: instability starts at the same β value, hence at larger depth for larger field, the growth rate is field independent. Taken from **Paper VII**.

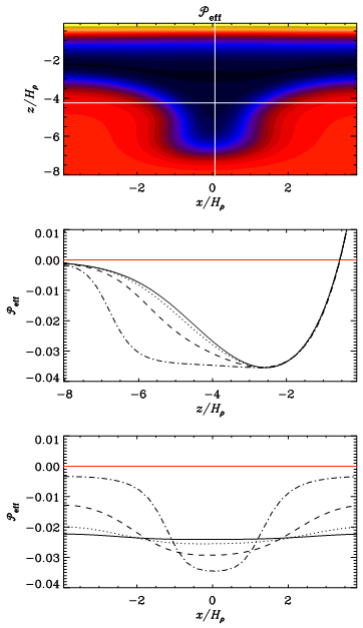

Figure 5.8: Effective magnetic pressure along the perpendicular directions at different times. Taken from **Paper VIII**.

change on the order of a few percent, much smaller than the turbulent perturbations and thus only discernible in mean-field simulations.

We see in figure 5.8 that the structures become progressively narrower and with β inside increasing towards β_{min}. As the density is higher deeper down, the field becomes larger than the originally imposed one.

As the background magnetic field gets depleted, no fields remain to be dragged along in the feedback mechanism. Thus inflows now only add density, reducing β and as such the pressure difference with the background. Without source the existing over-dense structure starts to sink.

5.4.5 Model extension (Paper VIII)

Our model reproduces the direct simulations rather well for the current setup. However, as we have structure formation the field is no longer constant. The effect of the presence of gradient terms of the magnetic field is assessed by including $\overline{\boldsymbol{J}}$ as a building block in the model (other magnetic gradient components are still zero). Thus we have to extend equation (5.7) to an expression of the form

$$\Delta\overline{\Pi}^{B}_{ij} = -\frac{1}{2}\left(\tilde{q}_B\overline{\boldsymbol{B}}^2 + \tilde{q}_J\overline{\boldsymbol{J}}^2 + \tilde{q}_g\boldsymbol{g}^2\right)\delta_{ij} + \tilde{q}_{Bs}\overline{B}_i\overline{B}_j + \tilde{q}_{Js}\overline{J}_i\overline{J}_j + \tilde{q}_{gs}g_ig_j, \quad (5.10)$$

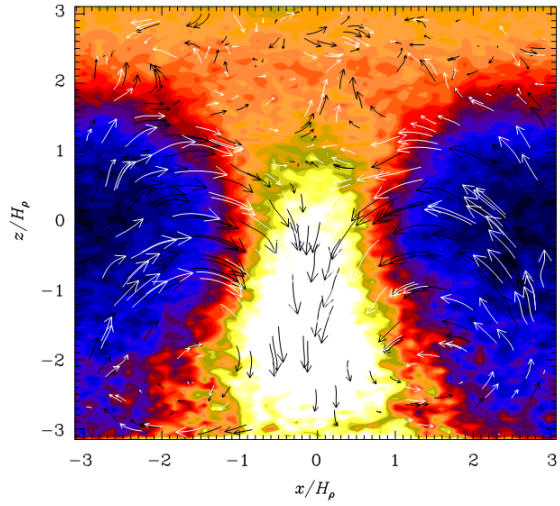

Figure 5.9: Flows in the nonlinear stage. High $\overline{B}$: inflows and sinking, low $\overline{B}$: outflows and buoyancy. Taken from **Paper VII**.

where the isotropic component is now in a more explicit form, and where $\tilde{q}_{Bs}$ and $\tilde{q}_{gs}$ map to q_s and q_g in equation (5.7); the coefficients themselves depend on the mean fields. A first impression from figure 5.10 is that the presence of currents increases the negative magnetic pressure effect.

If, in addition, we also allow some net helicity, combinations of $\overline{\boldsymbol{J}}$ and $\overline{\boldsymbol{B}}$ may have non-zero (pseudo-scalar) coefficients. If there is sufficient helicity there will also be an α effect generating a dynamo field. The interaction of NEMPI with such a field will be addressed in subsequent works. Also the effect of gravity, see figure 5.10, on the pressure reduction (q_g) is still to be properly investigated. Once these questions have been addressed and understood we can consider the energy equation. Note that the latter is already included in mean-field simulations by Käpylä et al. (2012).

5.5 NEMPI in the sun?

So how are we doing in terms of solar surface fields? We observe magnetic structures that are larger than the turbulent injection scale and that last longer than a turbulent turnover time. In the sun such a separation of scales between small granules and large magnetic structures is indeed observed. However, the length scales found in the simulations are of the order of the density scale height. The latter increases strongly with depth, hence 'getting it right' depends strongly on where the structures are formed. Likewise for the magnetic

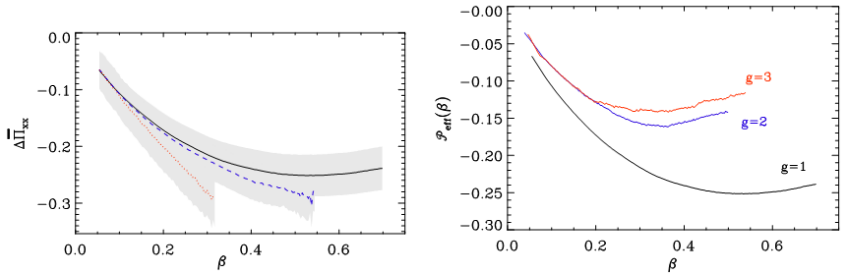

Figure 5.10: Changes in the diagonal components in the presence of currents (data was binned in points with no current (black), low current (blue) and high current (red). Reduction of the effect for increased gravity strengths. Taken from **Paper VIII**.

field, as this mechanism is limited to a fraction of the equipartition field, the maximal field strength (in absolute units) which can be reached increases with the depth of formation.

The growth rate during the linear stage, calculated for an isothermally stratified atmosphere, for velocities and length scales of the order of the ones observed at the solar surface, gives growth timescales of the order of days (**Paper VII**). How exactly the growth rate expression is translated to a convective atmosphere is unclear, and, as pointed out earlier, these input parameters vary quite strongly with depth. The timescales in the non-linear stage are mostly limited by the sinking of the structure. This sinking is indeed something we have to overcome to be able to produce any surface phenomena. It may be possible that this effect is reduced through interaction with the surface as a boundary or through the interaction with an instability originating in the energy equation (for example the one presented in Kitchatinov and Mazur, 2000).

Sinking might be avoided if the original field is regenerated through dynamo action, although, as mentioned before, the effect of helicity on the negative effective magnetic pressure effect is still to be properly investigated. This last point also ties to our somewhat artificial initial condition of a constant field, an assumption we would like to drop in the near future.

Epilogue

I would like to steal this last page to again point out the merits and limitations of the results presented in the included papers in terms of the quest for understanding the formation of sunspots.

It is clear that our current setup, isothermal stratification with forced turbulence rather than turbulent convection, and consequently an imposed field rather than a dynamo generated one, is too simplified to be compared directly with the solar convection zone.

However, we have now clearly demonstrated that the predicted turbulent pressure reduction in the presence of a weak magnetic field exists and may well persist for more solar like turbulence.

We have, for the first time, observed the instability due to this effect in direct numerical simulations. This instability is able to concentrate energy from a uniform background magnetic field into localised structures on spatial and temporal scales that are much larger than the ones associated with the (forced) turbulence. The behaviour of the instability (in the studied setup), found in direct simulations, agrees very well with the results from our current mean-field model.

The continuation of this work will first require a more detailed numerical and analytical study of higher order effects related to structure formation as we started in the last paper, as well as the effect of inclusion of forcing with a finite degree of helicity. When these are well understood, only more numerically expensive simulations with realistic (convective) forcing and (radiative) boundary conditions, will be able to provide further answers.

References

H. D. Babcock. The Sun's polar magnetic field. *Astrophys. J.*, 130:364, 1959. 4

H. W. Babcock. The topology of the Sun's magnetic field and the 22-year cycle. *Astrophys. J.*, 133:572, 1961. 27, 28

H. W. Babcock and H. D. Babcock. The Sun's magnetic field, 1952-1954. *Astrophys. J.*, 121:349, 1955. 4

N. Babkovskaia, N. E. L. Haugen, and A. Brandenburg. A high-order public domain code for direct numerical simulations of turbulent combustion. *Journal of Computational Physics*, 230:1–12, 2011. 24

H. Balthasar, M. Vazquez, and H. Wöhl. Differential rotation of sunspot groups in the period from 1874 through 1976 and changes of the rotation velocity within the solar cycle. *Astron. Astrophys.*, 155:87–98, 1986. 30

E. G. Blackman and G. B. Field. Constraints on the magnitude of α in dynamo theory. *Astrophys. J.*, 534: 984–988, 2000. 19

A. Brandenburg. The case for a distributed solar dynamo shaped by near-surface shear. *Astrophys. J.*, 625: 539–547, 2005. 31

A. Brandenburg and K. Subramanian. Strong mean field dynamos require supercritical helicity fluxes. *Astron. Nachr.*, 326:400–408, 2005. 19

A. Brandenburg, K.-H. Rädler, and M. Schrinner. Scale dependence of alpha effect and turbulent diffusivity. *Astron. Astrophys.*, 482:739–746, 2008. 18

A. Brandenburg, N. Kleeorin, and I. Rogachevskii. Large-scale magnetic flux concentrations from turbulent stresses. *Astron. Nachr.*, 331:5, 2010. 33, 35

R. C. Carrington. On the distribution of the solar spots in latitudes since the beginning of the year 1854, with a map. *Month. Not. Roy. Astron. Soc.*, 19:1–3, 1858. 1

M. C. M. Cheung, M. Rempel, A. M. Title, and M. Schüssler. Simulation of the Formation of a Solar Active Region. *Astrophys. J.*, 720:233–244, 2010. 30

A. R. Choudhuri and P. A. Gilman. The influence of the Coriolis force on flux tubes rising through the solar convection zone. *Astrophys. J.*, 316:788–800, 1987. 28

J. Christensen-Dalsgaard. Lecture notes on stellar oscillations. 2003. 6

J. Christensen-Dalsgaard, D. Gough, and J. Toomre. Seismology of the Sun. *Science*, 229:923–931, 1985. 5

J. Christensen-Dalsgaard, D. O. Gough, and M. J. Thompson. The depth of the solar convection zone. *Astrophys. J.*, 378:413–437, 1991. 7

R. Courant, K. Friedrichs, and H. Lewy. Über die partiellen Differenzengleichungen der mathematischen Physik. *Mathematische Annalen*, 100:32–74, 1928. 22

S. D'Silva and A. R. Choudhuri. A theoretical model for tilts of bipolar magnetic regions. *Astron. Astrophys.*, 272:621, 1993. 30

J. A. Eddy. The Maunder minimum. *Science*, 192:1189–1202, 1976. 5

Y. Fan. Magnetic fields in the solar convection zone. *Living Reviews in Solar Physics*, 6:4, 2009. 9

Y. Fan, W. P. Abbett, and G. H. Fisher. The dynamic evolution of twisted magnetic flux tubes in a three-dimensional convecting flow. I. Uniformly buoyant horizontal tubes. *Astrophys. J.*, 582:1206–1219, 2003. 27

G. Galilei. Istoria e dimostrazioni intorno alle macchie solari. 1613. 2

G. Guerrero and P. J. Käpylä. Dynamo action and magnetic buoyancy in convection simulations with vertical shear. *Astron. Astrophys.*, 533:A40, 2011. 29

G. E. Hale. On the probable existence of a magnetic field in sun-spots. *Astrophys. J.*, 28:315, 1908. 3

G. E. Hale, F. Ellerman, S. B. Nicholson, and A. H. Joy. The magnetic solarity of sun-spots. *Astrophys. J.*, 49:153, 1919. 4

D. H. Hathaway. Doppler measurements of the Sun's meridional flow. *Astrophys. J.*, 460:1027, 1996. 3

D. H. Hathaway. The solar cycle. *Living Reviews in Solar Physics*, 7, 2010. 5

T. Heinemann, W. Dobler, Å. Nordlund, and A. Brandenburg. Radiative transfer in decomposed domains. *Astron. Astrophys.*, 448:731–737, 2006. 24

R. Howe. Solar interior rotation and its variation. *Living Reviews in Solar Physics*, 6:1, 2009. 8

D. V. Hoyt and K. H. Schatten. Group sunspot numbers: a new solar activity reconstruction. *Sol. Phys.*, 179:189–219, 1998. 6

H. Ji and S. C. Prager. The α dynamo effects in laboratory plasmas. *Magnetohydrodynamics*, 38:191–210, 2002. 19

A. Johansen, J. S. Oishi, M.-M. Mac Low, H. Klahr, T. Henning, and A. Youdin. Rapid planetesimal formation in turbulent circumstellar disks. *Nature*, 448:1022–1025, 2007. 24

P. J. Käpylä, A. Brandenburg, N. Kleeorin, M. J. Mantere, and I. Rogachevskii. Negative effective magnetic pressure in turbulent convection. *Month. Not. Roy. Astron. Soc.*, 422:2465–2473, 2012. 35, 42

A. P. Kazantsev. Enhancement of a magnetic field by a conducting fluid. *Sov. J. Exp. Theor. Phys.*, 26:1031, 1968. 16

A. P. Kazantsev, A. A. Ruzmaikin, and D. D. Sokolov. Magnetic field transport by an acoustic turbulence-type flow. *Zhurnal Eksperimental noi i Teoreticheskoi Fiziki*, 88:487–494, 1985. 16

L. L. Kitchatinov and M. V. Mazur. Stability and equilibrium of emerged magnetic flux. *Sol. Phys.*, 191: 325–340, 2000. 32, 43

I. N. Kitiashvili, A. G. Kosovichev, A. A. Wray, and N. N. Mansour. Mechanism of spontaneous formation of stable magnetic structures on the Sun. *Astrophys. J.*, 719:307–312, 2010. 32

N. Kleeorin and I. Rogachevskii. Effective Ampère force in developed magnetohydrodynamic turbulence. *Phys. Rev. E*, 50:2716–2730, 1994. 32

N. Kleeorin and A. Ruzmaikin. Dynamics of the average turbulent helicity in a magnetic field. *Magneto-hydrodynamics*, 18:116–122, 1982. 19

N. Kleeorin, I. Rogachevskii, and A. Ruzmaikin. Magnetic force reversal and instability in a plasma with developed magnetohydrodynamic turbulence. *Sov. Phys. JETP*, 70:878–883, 1990. 32

N. Kleeorin, D. Moss, I. Rogachevskii, and D. Sokoloff. Helicity balance and steady-state strength of the dynamo generated galactic magnetic field. *Astron. Astrophys.*, 361:L5–L8, 2000. 19

N. I. Kleeorin, I. V. Rogachevskii, and A. A. Ruzmaikin. The effect of negative magnetic pressure and the large-scale magnetic field instability in the solar convective zone. *Pisma Astron. Zh.*, 15:639–645, 1989. 9, 32

A. Kolmogorov. The local structure of turbulence in incompressible viscous fluid for very large Reynolds' numbers. *Akademiia Nauk SSSR Doklady*, 30:301–305, 1941. 12

A. G. Kosovichev. Tomographic imaging of the Sun's interior. *Astrophys. J. Lett.*, 461:L55, 1996. 5

A. G. Kosovichev and J. O. Stenflo. Tilt of emerging bipolar magnetic regions on the Sun. *Astrophys. J. Lett.*, 688:L115–L118, 2008. 30

F. Krause and K.-H. Rädler. *Mean-field magnetohydrodynamics and dynamo theory*. Pergamon Press, Ltd., Oxford, 1980. 16

J. H. Lienhard. *Synopsis of lift, drag, and vortex frequency data for rigid circular cylinders.* Washington State University, 1966. 13

M. G. Linton, D. W. Longcope, and G. H. Fisher. The helical kink instability of isolated, twisted magnetic flux tubes. *Astrophys. J.*, 469:954, 1996. 27

D. W. Longcope, G. H. Fisher, and S. Arendt. The evolution and fragmentation of rising magnetic flux tubes. *Astrophys. J.*, 464:999, 1996. 27

V. Martinez Pillet, B. W. Lites, and A. Skumanich. Active region magnetic fields. I. Plage fields. *Astrophys. J.*, 474:810, 1997. 4

H. K. Moffatt. *Magnetic field generation in electrically conducting fluids*. Cambridge University Press, 1978. 16

NASA/Marshall solar Physics. http://solarscience.msfc.nasa.gov. 2

Å. Nordlund, A. Brandenburg, R. L. Jennings, M. Rieutord, J. Ruokolainen, R. F. Stein, and I. Tuominen. Dynamo action in stratified convection with overshoot. *Astrophys. J.*, 392:647–652, 1992. 29

Å. Nordlund, R. F. Stein, and M. Asplund. Solar surface convection. *Living Reviews in Solar Physics*, 6:2, April 2009. 8

S. Ortolani and D. Schnack. *Magnetohydrodynamics of plasma relaxation*. World Scientific Publishing, Co. Pte. Ltd., Singapore, 1993. 19

E. N. Parker. The formation of sunspots from the solar toroidal field. *Astrophys. J.*, 121:491, 1955. 27

E. N. Parker. The generation of magnetic fields in astrophysical bodies. X - Magnetic buoyancy and the solar dynamo. *Astrophys. J.*, 198:205–209, 1975. 28

E. N. Parker. Sunspots and the physics of magnetic flux tubes. I - The general nature of the sunspot. II - Aerodynamic drag. *Astrophys. J.*, 230:905–923, 1979. 27

J. Peiró and S. Sherwin. Finite difference, finite element and finite volume methods for partial differential equations. In Yip S., editor, *Handbook of materials modeling, Vol. 1: Methods and models*, pages 1–32. Springer, Berlin, 2005. 21

PENCIL CODE. https://code.google.com/p/pencil-code, 2001. 21

A. Pouquet, U. Frisch, and J. Leorat. Strong MHD helical turbulence and the nonlinear dynamo effect. *Journal of Fluid Mechanics*, 77:321–354, 1976. 19

W. H. Press, S. A. Teukolsky, W. T. Vetterling, and B. P. Flannery. *Numerical recipes in FORTRAN. The art of scientific computing*. Cambridge University Press, 1992. 21

M. Rheinhardt and A. Brandenburg. Test-field method for mean-field coefficients with MHD background. *Astron. Astrophys.*, 520:A28, 2010. 18

M. Rheinhardt and A. Brandenburg. Modeling spatio-temporal nonlocality in mean-field dynamos. *Astron. Nachr.*, 333:71–77, 2012. 18

L. F. Richardson. *Weather prediction by numerical process*. Cambridge University Press, 1922. 12

M. Rieutord and F. Rincon. The Sun's supergranulation. *Living Reviews in Solar Physics*, 7:2, 2010. 3

I. Rogachevskii and N. Kleeorin. Magnetic fluctuations and formation of large-scale inhomogeneous magnetic structures in a turbulent convection. *Phys. Rev. E*, 76(5):056307, 2007. 32

Royal Swedish Academy of Sciences. http://www.solarphysics.kva.se. 2

A. Ruzmaikin. Clustering of emerging magnetic flux. *Sol. Phys.*, 181:1–12, 1998. 28

A. A. Schekochihin, S. C. Cowley, S. F. Taylor, J. L. Maron, and J. C. McWilliams. Simulations of the small-Scale turbulent dynamo. *Astrophys. J.*, 612:276–307, 2004. 16

M. Schrinner, K.-H. Rädler, D. Schmitt, M. Rheinhardt, and U. Christensen. Mean-field view on rotating magnetoconvection and a geodynamo model. *Astron. Nachr.*, 326:245–249, 2005. 17

M. Schrinner, K.-H. Rädler, D. Schmitt, M. Rheinhardt, and U. R. Christensen. Mean-field concept and direct numerical simulations of rotating magnetoconvection and the geodynamo. *Geophysical and Astrophysical Fluid Dynamics*, 101:81–116, 2007. 17

M. Schwabe. Sonnenbeobachtungen im Jahre 1843. Von Herrn Hofrath Schwabe in Dessau. *Astron. Nachr.*, 21:233, 1844. 1

SDO/HMI. http://sdo.gsfc.nasa.gov. 3

S. K. Solanki. Sunspots: an overview. *Astron. Astrophys. Rep.*, 11:153–286, 2003. 4

F. W. G. Spörer. Resultate aus Beobachtungen der Sonnenflecken. *Astron. Nachr.*, 107:331, 1883. 1

H. C. Spruit. Pressure equilibrium and energy balance of small photospheric fluxtubes. *Sol. Phys.*, 50: 269–295, 1976. 32

M. Steenbeck, F. Krause, and K.-H. Rädler. Berechnung der mittleren Lorentz-Feldstärke $v \times B$ für ein elektrisch leitendes Medium in turbulenter, durch Coriolis-Kräfte beeinflußter Bewegung. *Zeitschrift Naturforsch. A*, 21:369, 1966. 16

R. F. Stein and Å. Nordlund. On the formation of active regions. *Astrophys. J. Lett.*, 753:L13, 2012. 31

J. O. Stenflo and A. G. Kosovichev. Bipolar magnetic regions on the Sun: global analysis of the SOHO/MDI data set. *Astrophys. J.*, 745:129, 2012. 30

M. Stix. *The Sun. An introduction*. Springer-Verlag, Berlin, 1989. 1, 7

M. J. Thompson, J. Christensen-Dalsgaard, M. S. Miesch, and J. Toomre. The internal rotation of the Sun. *Ann. Rev. Astron. Astrophys.*, 41:599–643, 2003. 30

S. M. Tobias, N. H. Brummell, T. L. Clune, and J. Toomre. Pumping of magnetic fields by turbulent penetrative convection. *Astrophys. J. Lett.*, 502:L177, 1998. 29

I. G. Usoskin. A history of solar activity over millennia. *Living Reviews in Solar Physics*, 5:3, 2008. 6

J. M. Vaquero and M. Vázquez, editors. *The Sun recorded through history: scientific data extracted from historical documents*, volume 361 of *Astrophysics and Space Science Library*, 2009. 1

M. A. Weber, Y. Fan, and M. S. Miesch. Comparing simulations of rising flux tubes through the solar convection zone with observations of solar active regions: constraining the dynamo field strength. *Solar Physics*, 2012. 30

J. A. Westwood Oliver. *Sunspottery: Or, What do we owe to the Sun?* Simpkin, Marshall, London, 1883. 1

J. H. Williamson. Low-storage Runge-Kutta schemes. *Journal of Computational Physics*, 35:48, 1980. 22

S. Yashiro and K. Shibata. Relation between thermal and magnetic properties of active regions as a probe of coronal heating mechanisms. *Astrophys. J. Lett.*, 550:L113–L116, 2001. 4

I. B. Zeldovich, A. A. Ruzmaikin, and D. D. Sokolov. *Magnetic fields in astrophysics*, volume 3. New York, Gordon and Breach Science Publishers, 1983. 17

Y. B. Zeldovich, A. A. Ruzmaikin, and D. D. Sokoloff. *The almighty chance*. World Scientific Publication, Singapore, 1990. 16

J. Zhao, A. G. Kosovichev, and T. L. Duvall, Jr. Investigation of mass flows beneath a sunspot by time-distance helioseismology. *Astrophys. J.*, 557:384–388, 2001. 9